Particles and the Cosmos

2020/2021

Sascha Caron, Jörg Hörandel

NM109
first semester, 6 ec

28 hrs lecture Tuesday 8:30 - 10:15
28 hrs problem session Wednesday 10:30 - 12:15

Lectures:

Experimental methods (JRH)
01.09.2020 1. Interactions with matter
08.09.2020 2. Detectors

Standard model (SC)
15.09.2020 3. Particles, QED, Feynman rules
22.09.2020 4. Hadrons and QCD
29.09.2020 5. Hadrons and QCD
06.10.2020 6. Weak interactions, CP violation
13.10.2020 7. Higgs mechanism

Astroparticle physics (JRH)
03.11.2020 8. The birth of cosmic rays
10.11.2020 9. Cosmic rays in the Galaxy, in the heliosphere, and the Earth magnetic field
17.11.2020 10. Cosmic rays at the top of and in the atmosphere
24.11.2020 11. Cosmic rays underground - neutrino oscillations
01.12.2020 12. Neutrino oscillations

Beyond the Standard Model, Dark Matter (SC)
08.12.2020 13. Lambda CDM, Big-bang nucleosynthesis
15.12.2020 14. Dark matter - Beyond-the-standard-model reasons

for Astroparticle Physics

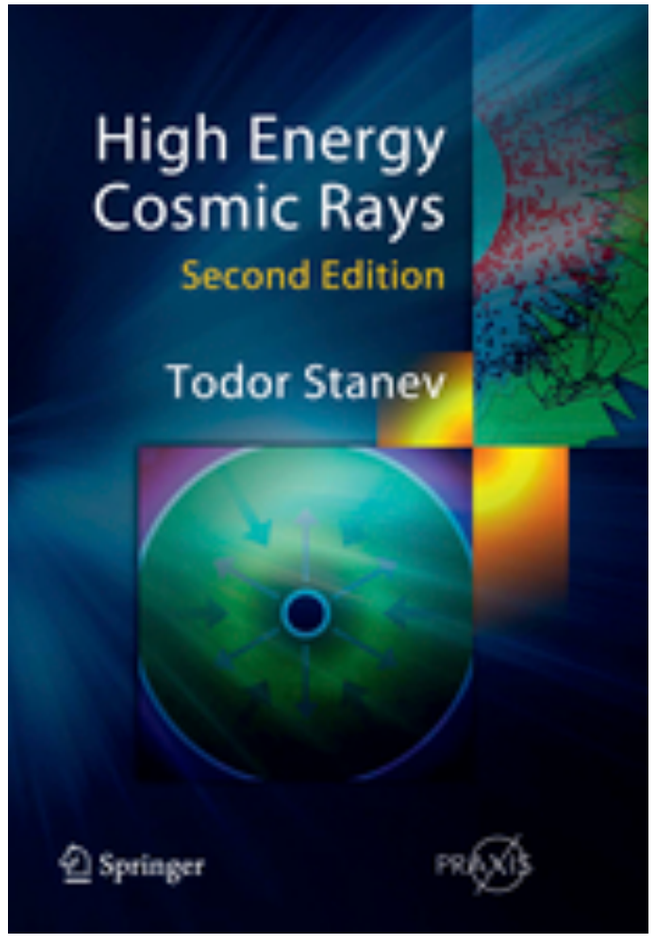

Jörg R. Hörandel
HG 02.728
http://particle.astro.ru.nl

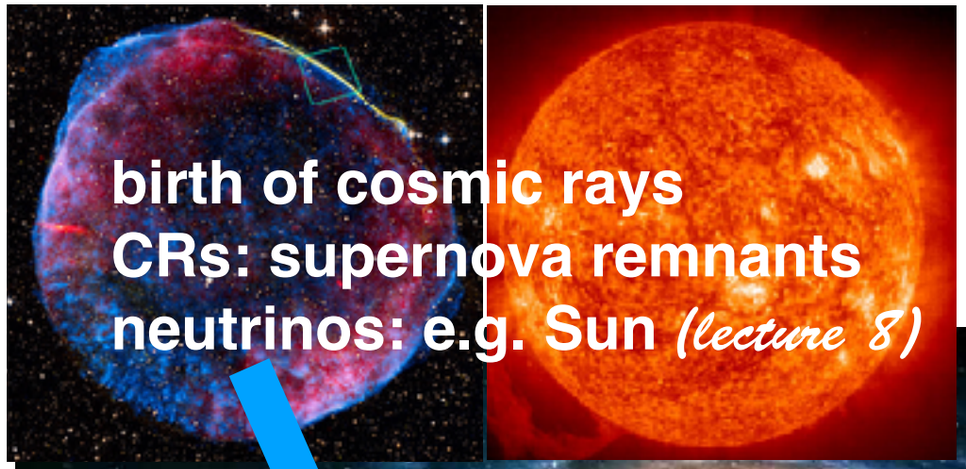

birth of cosmic rays
CRs: supernova remnants
neutrinos: e.g. Sun *(lecture 8)*

propagation of CRs in the Galaxy
interactions with ISM *(lecture 9)*

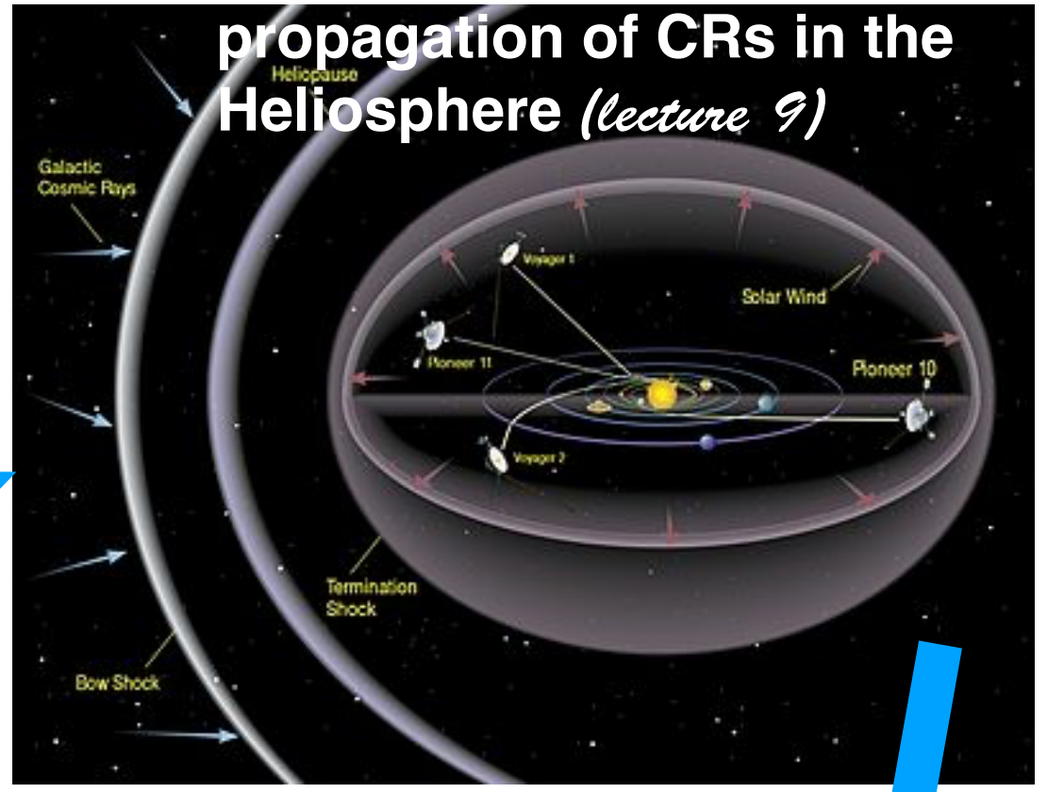

propagation of CRs in the Heliosphere *(lecture 9)*

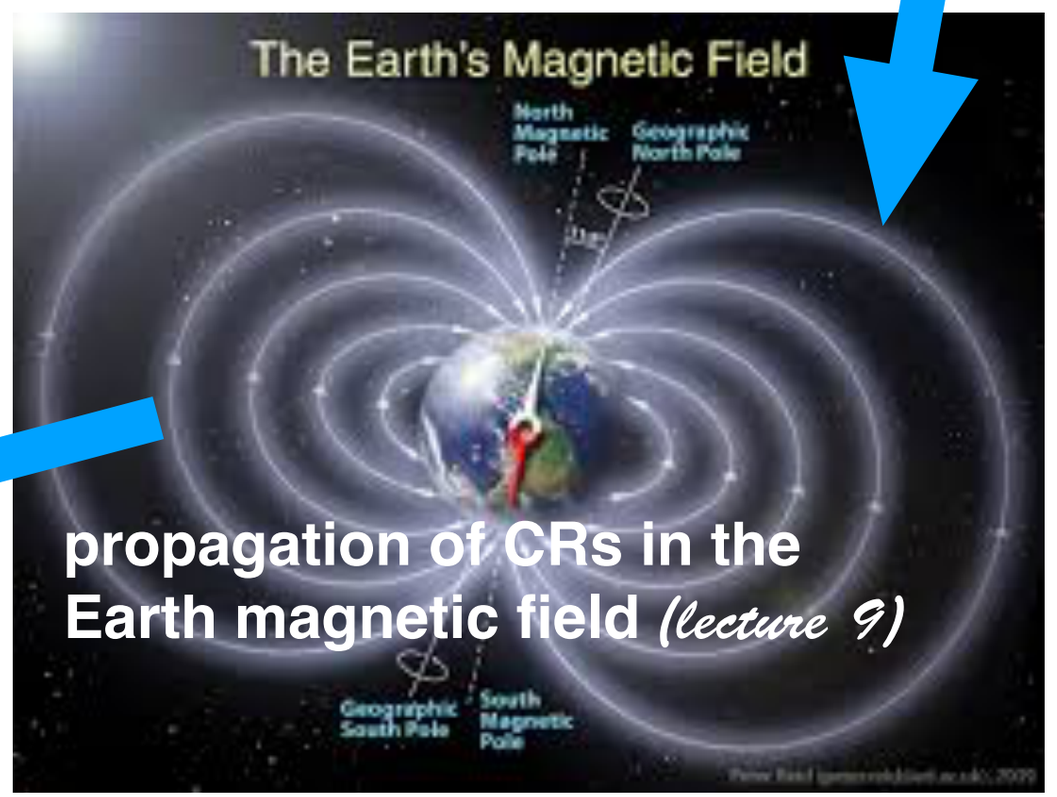

propagation of CRs in the Earth magnetic field *(lecture 9)*

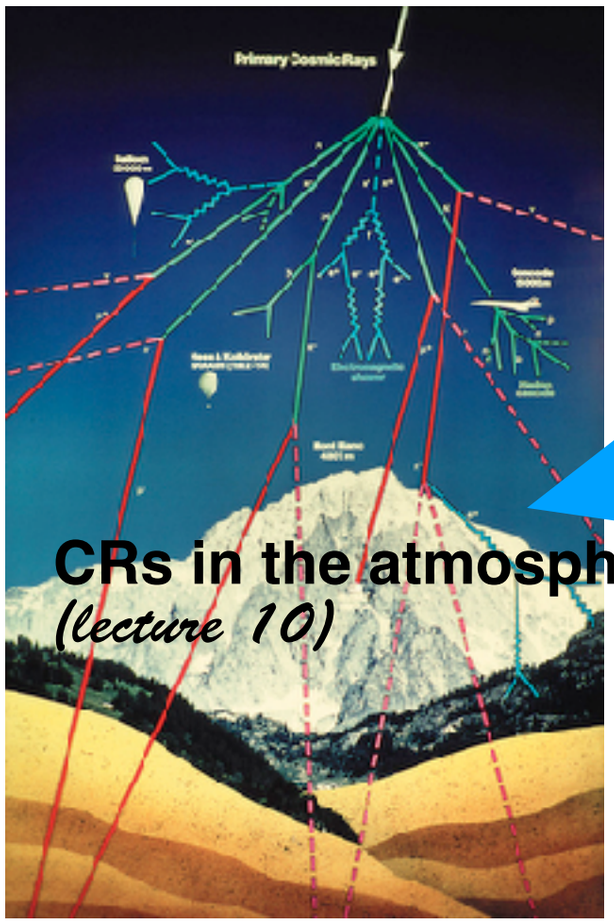

CRs in the atmosphere
(lecture 10)

CRs at the top of the atmosphere *(lecture 10)*

CRs underground *(lecture 11)*
neutrino oscillations *(lecture 11+12)*

today:
Stanev, chapter 7

7 Cosmic rays underground 137
7.1 High energy muons underground 138
7.2 Atmospheric neutrinos 146
7.2.1 Upward-going muons 151
7.2.2 Flux calculations 155
7.2.3 Experimental data 159
7.3 Neutrino oscillations 162
7.3.1 Matter effects 164
7.3.2 Oscillation parameters 165

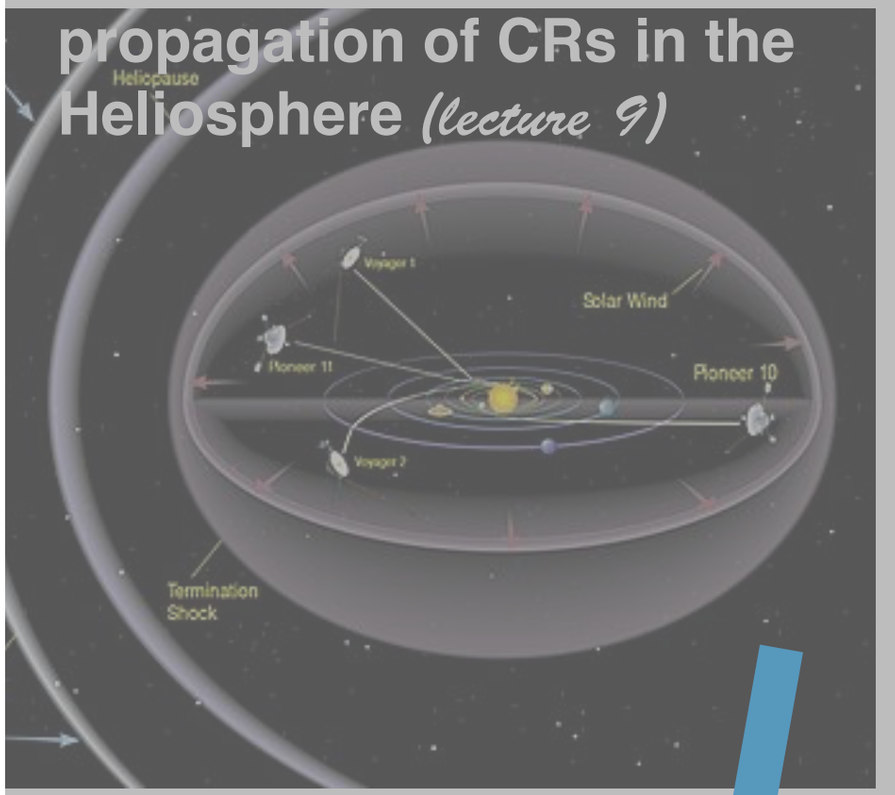

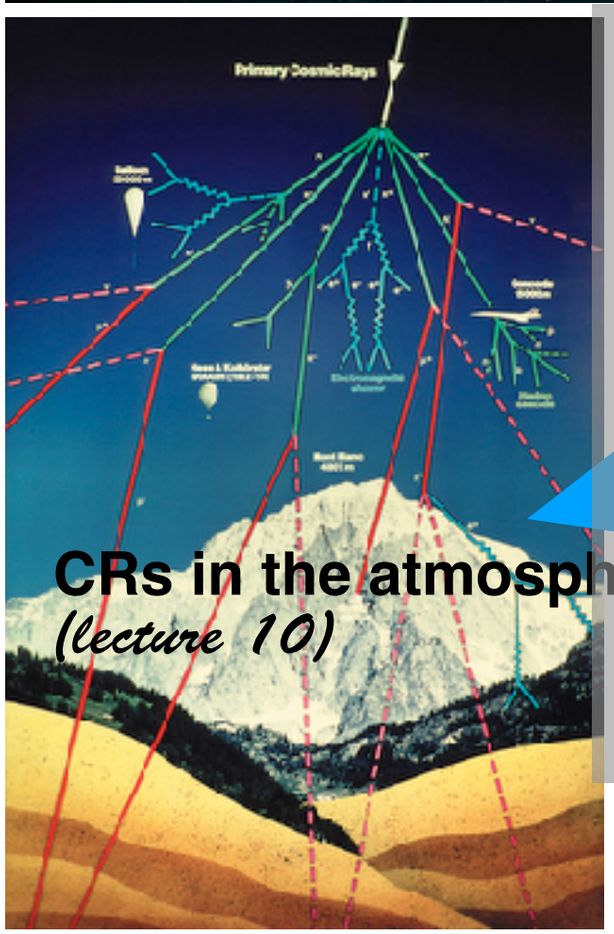

CRs in the atmosphere
(lecture 10)

CRs at the top of the
atmosphere (lecture 10)

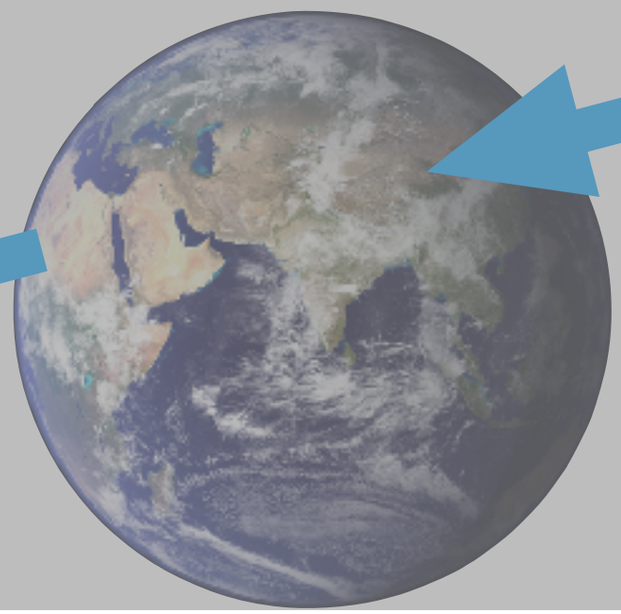

CRs underground (lecture 11)
neutrino oscillations (lecture 11+12)

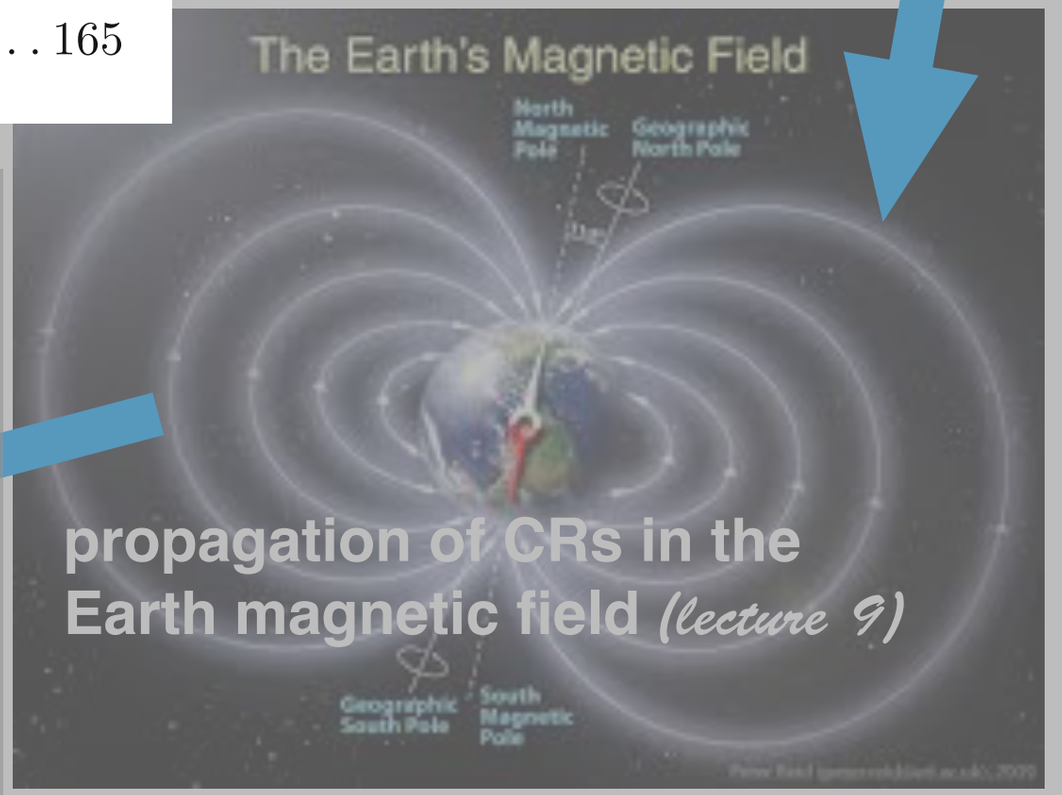

Cosmic rays underground

primary cosmic rays almost never reach sea level
atmosphere is ~12 hadronic interaction lengths thick $\lambda_p(air) = 80\ \mathrm{g/cm^2}$

$$1030\ \mathrm{g/cm^2}/80\ \mathrm{g/cm^2} \approx 12$$

probability of primary cosmic ray to survive $\approx \exp(-12) \approx 6 \cdot 10^{-6}$

be careful, in the literature the term „secondary cosmic rays“ is used two-fold:
in the Galaxy, secondary CRs are produced in spallation reactions, e.g. Li, Be, B
in the atmosphere CRs produce secondary particles such as pions, muons, etc

secondary particles produced in the atmosphere reach sea level
hadrons, electrons and gamma rays interact immediately with the rock and are quickly absorbed
10 m of rock provide two or three times more column density than the whole atmosphere
only high-energy muons (E>500 GeV) can penetrate deep underground
also neutrinos (with their small interaction cross section) can penetrate many meters of rock

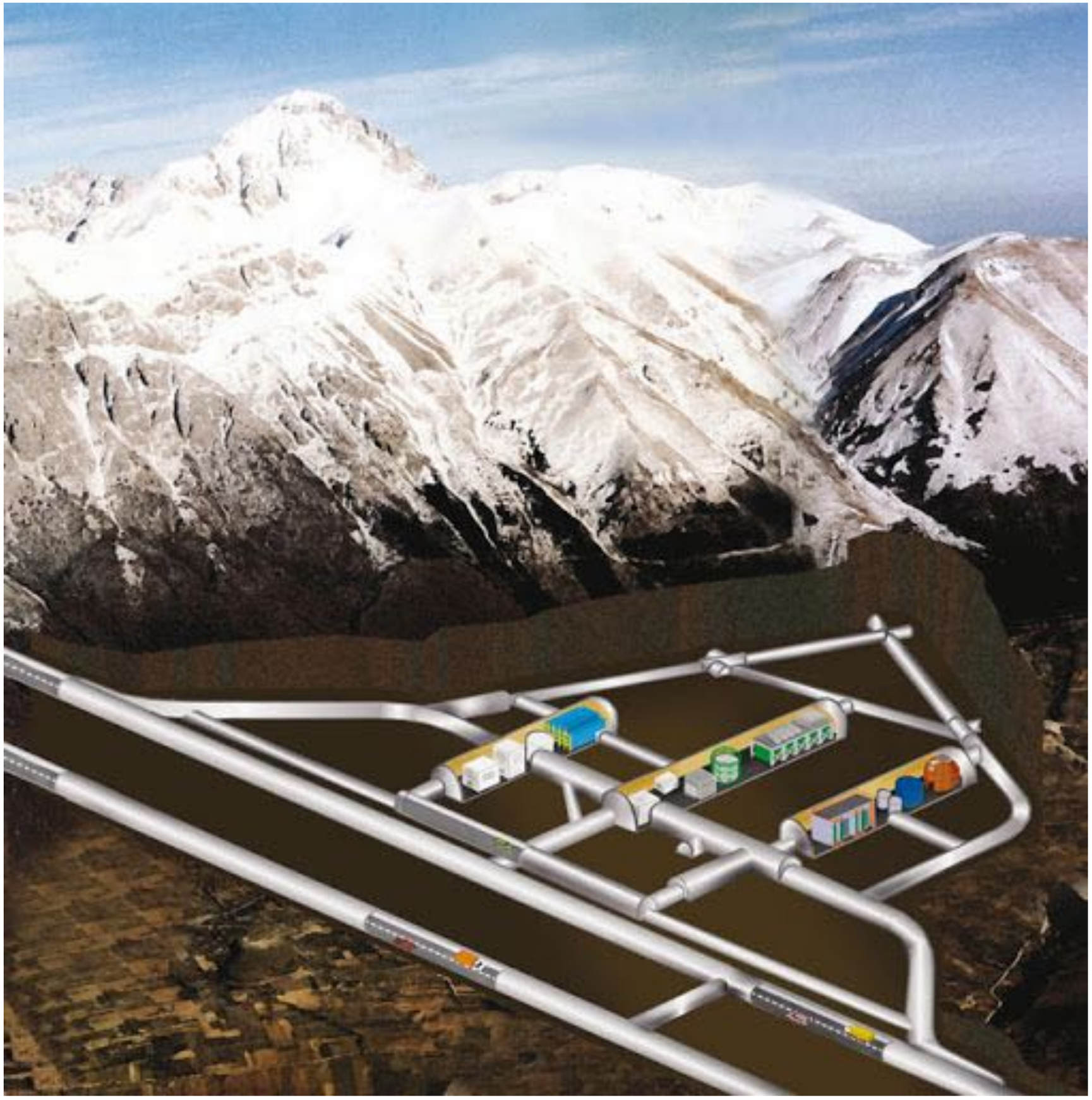

Laboratori Nazionali del Gran Sasso

High energy muons underground

For the GeV muons discussed in Chap. 6 the only essential energy loss process is ionization. The reason is that the atmospheric depth is vertically only 1,000 g/cm^2. For the muons underground, however, other processes become increasingly important. Imagine a laboratory 1 km underground. For the average density of the upper crust of the Earth of 2.65 g/cm^3 the column depth is 2.65×10^5 g/cm^2. Because the rock density for experiments at different locations varies, it is often measured in kilometers of water equivalent (1 k.w.e. = 10^5 g/cm^2). At such depths other muon energy loss processes become important. These are the radiation processes of bremsstrahlung, direct pair-production, and photoproduction. Direct pair-production is a process in which the muon emits a virtual photon and the virtual photon produces an electron–positron pair. Because of the two electromagnetic vertices the cross-section is proportional to α^2, not to α as for bremsstrahlung, and is thus smaller by a factor of 100. Photoproduction is also related to the emission of a virtual photon. In this case the photon interacts hadronically with matter and generates secondary hadrons. Since the generation of a pion requires center of mass energy at least equal to the sum of the proton and pion masses, only higher energy virtual photons are important and the cross-section at muon energies in the GeV range is very small.

High energy muons underground

Ionization energy loss depends only weakly on the muon energy and in first approximation can be considered constant at about 2 MeV per g/cm^2. Radiation processes on the other hand cause energy loss that is proportional to the muon energy, i.e. $dE_\mu/dx = -bE_\mu$. The total muon energy loss then is

$$\frac{dE_\mu}{dx} = -a - bE_\mu \,, \tag{7.1}$$

where $b = b_{br} + b_{pair} + b_{ph}$ is the sum of the fractional energy loss in the three radiation processes. For rock b is roughly 4×10^{-6}. The critical energy for muons is the energy ϵ at which ionization energy loss equals radiation energy loss, i.e. $\epsilon = a/b \simeq 500$ GeV. The energy loss is dominated by radiation at $E_\mu \gg \epsilon$ and by ionization at $E_\mu \ll \epsilon$. These simple formulae let us calculate the average energy E_μ of a muon with initial energyE^0_μ after propagating through X g/cm^2 of rock

$$E_\mu = (E^0_\mu + \epsilon) \times \exp(-bX) - \epsilon \tag{7.2}$$

and the reverse quantity

$$E^0_\mu = (E_\mu + \epsilon) \times \exp(bX) - \epsilon \,. \tag{7.3}$$

High energy muons underground

The minimum energy for a muon to penetrate at depth X can be obtained from (7.3) when we set E_μ to 0, i.e.

$$E_\mu^{min} = \epsilon \left[\exp(bX) - 1\right] . \tag{7.4}$$

At small column depths, $X \ll 1/b$ g/cm^2 muons lose energy mostly on ionization and $E_\mu^{min} \simeq aX$. The muon energy spectrum underground then reflects the surface muon spectrum with a flattening under $E_\mu \simeq aX$. At big depths, $X \gg 1/b$ g/cm^2, the spectrum has almost constant shape up to $E_\mu \simeq \epsilon$ and steepens above that energy.

High energy muons underground

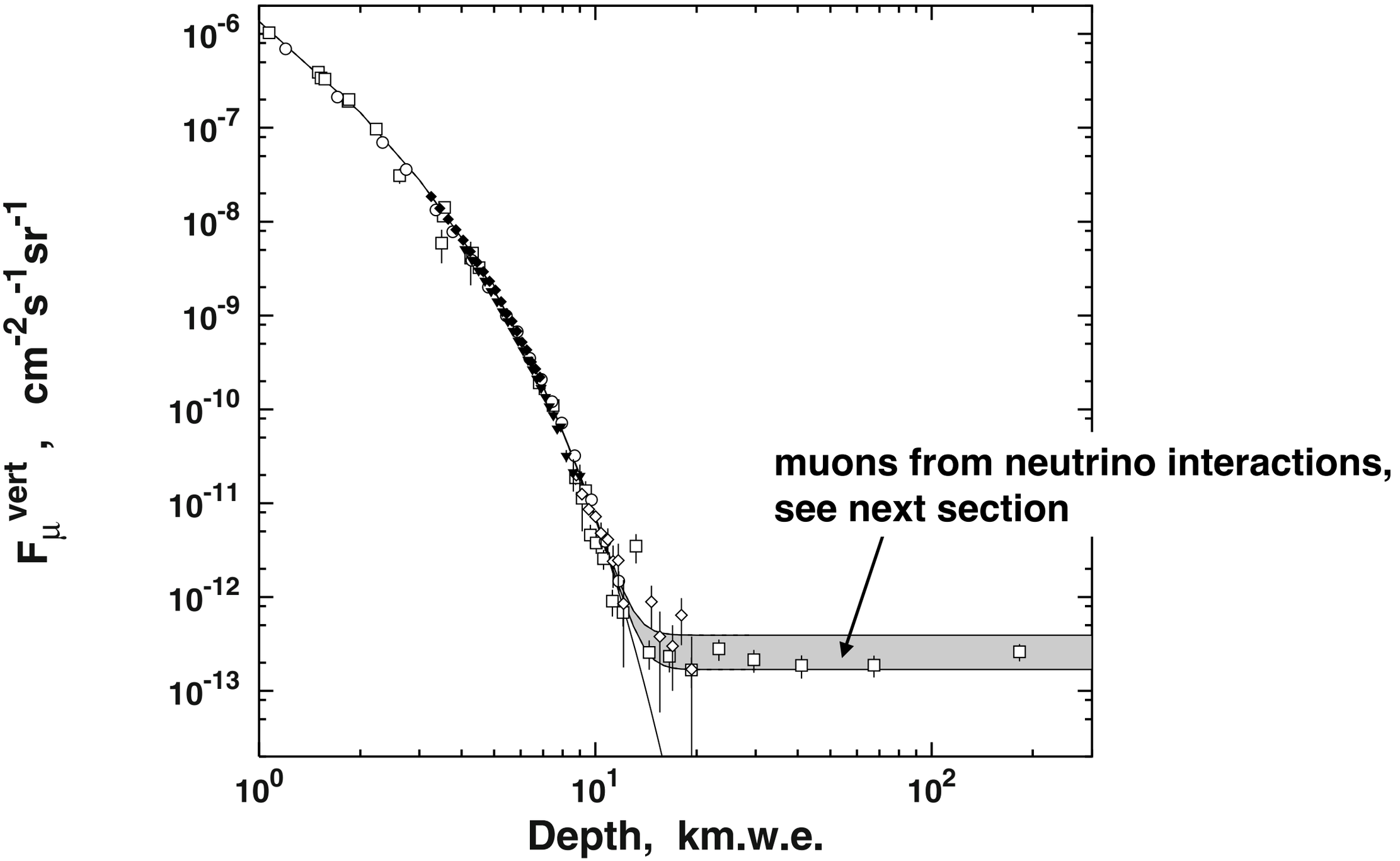

Fig. 7.1. Depth–intensity relation – the integral muon flux measured at different depths and angles and converted to vertical muon flux is compared to predictions. See text for the references to different data sets.

High energy muons underground

One can qualitatively understand the shape of the depth intensity curve if one assumes a power law muon energy spectrum on the ground $E_\mu = K E_\mu^{-\alpha}$ and accepts the definition of the minimum muon energy reaching depth X as in (7.4). The depth intensity relation then becomes

$$F_\mu^{vert} = \frac{K\,\epsilon^{-\alpha+1}}{\alpha-1} \times \exp(-(\alpha-1)bX) \times (1-e^{-bX})^{-\alpha+1}\,. \qquad (7.5)$$

The first term is a constant with depth and reflects the muon energy spectrum on the ground. The third one is always larger than 1 and approaches unity at large depths. At large depths the second term determines the depth intensity curve which has the exponential shape $\exp(-X/X_0)$ with $X_0 = [b(\alpha-1)]^{-1}$ as seen for large depths in Fig. 7.1. Since this asymptotic behavior is reached from above, the curve has a curvature at depths below ~10 km.w.e.

High energy muons underground

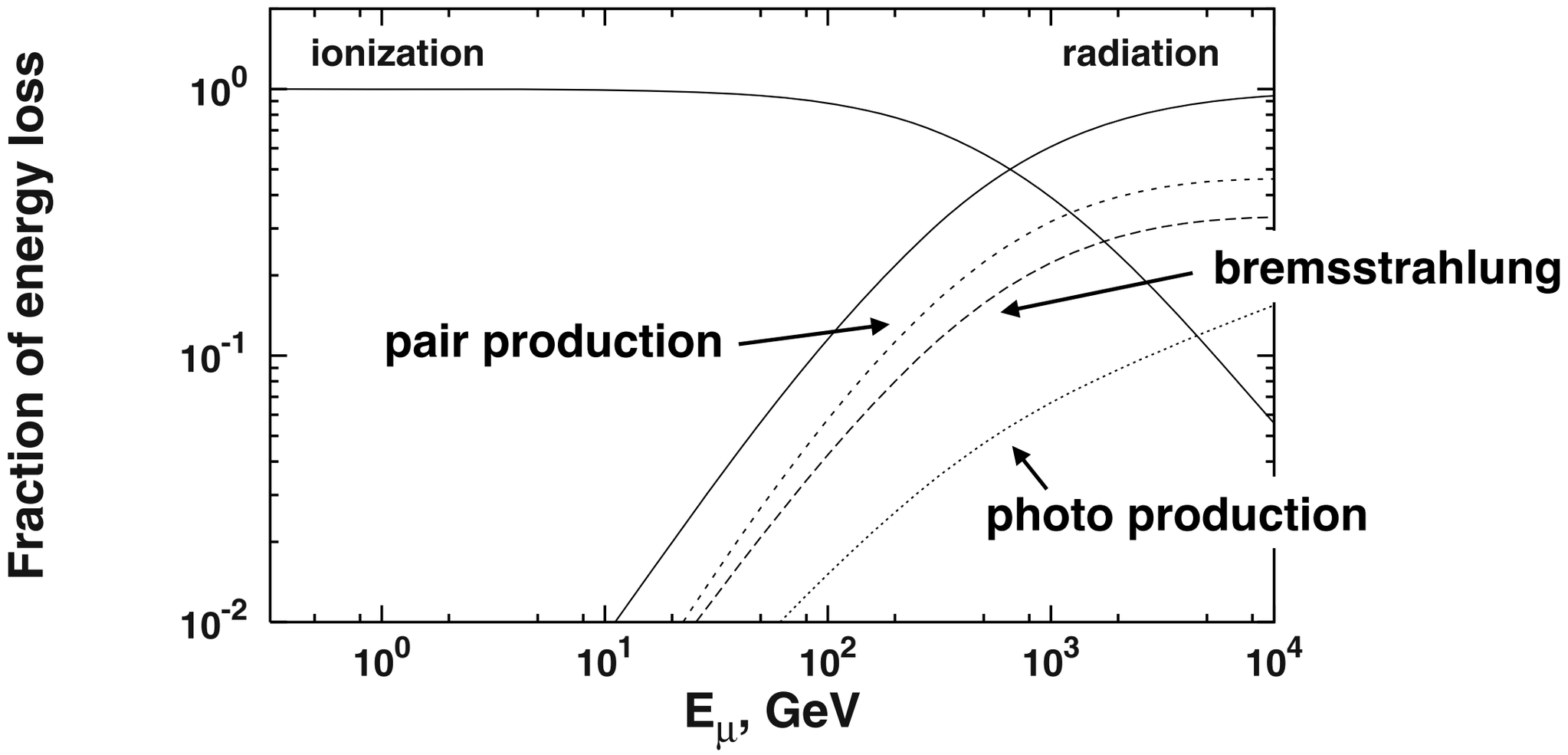

Fig. 7.2. Relative importance of different radiation processes as a function of the muon energy normalized to the total energy loss per g/cm^2. The long-dashed curve is for bremsstrahlung, the short-dashed curve for direct pair-production, and the dotted curve for photoproduction.

Muon propagation

It is easy to calculate the depth to which a muon can penetrate in the analytic presentation of the muon energy loss of (7.1). From (7.4) we obtain the range of a muon of energy E_μ, i.e. the underground depth that this muon will reach, as

$$R(E_\mu) \;=\; \frac{1}{b}\,\ln\left(\frac{E_\mu}{\epsilon}+1\right)\,. \tag{7.6}$$

The range of a muon of energy E_μ to be detected with certain nonzero energy can be obtained in a similar way from (7.3).

These expressions are good under the assumption of (7.1) – that the muon energy loss is continuous and that muons lose equal amount of energy in propagating through 1 g/cm^2 of matter. This is approximately true when ionization is the main energy loss process – up to 100 GeV as shown in Fig. 7.2. At higher energy the muon energy loss is not continuous - muons occasionally interact and lose a relatively large fraction of their energy. Fluctuations are inherent to the radiative processes and they replace the range $R(E_\mu)$ with a distribution of ranges.

—> survival probability for muons in standard rock

Muon propagation

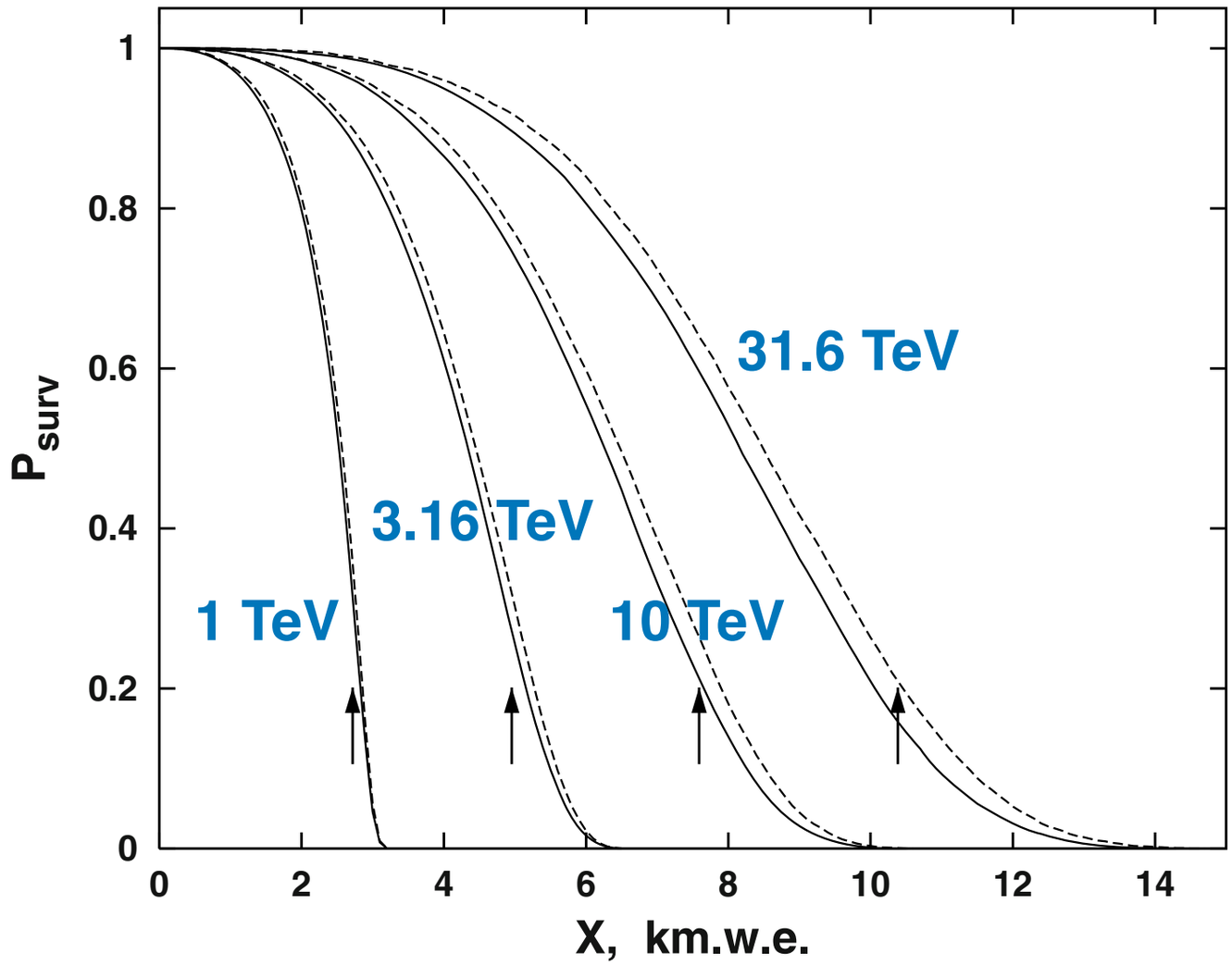

Fig. 7.3. Survival probability of muons with energy of 1., 3.16, 10., and 31.6 TeV in standard rock. The two curves for each energy indicate the uncertainties in the bremsstrahlung cross-section as stated in below. The arrows show the average depth for muon survival calculated from (7.4).

Muon propagation

The detection rate of muons at a certain depth X is

$$\int dN/dE_\mu P_{surv}(E_\mu, X)\, dE_\mu \,,$$

where P_{surv} is the muon survival probability at depth X. The effective muon range $R_{eff} \equiv \langle R_\mu \rangle$ is calculated as an integral over the survival probability.

$$R_{eff} = \int_0^\infty P_{surv}(E_\mu, X)\, dX \tag{7.7}$$

and can also be defined as the range for reaching depth X with energy higher than 0 using the calculated muon energy distribution instead of (7.3).

Cosmic rays underground

Stanev chapter 7

7 Cosmic rays underground 137
7.1 High energy muons underground 138
7.2 Atmospheric neutrinos 146
7.2.1 Upward-going muons 151
7.2.2 Flux calculations 155
7.2.3 Experimental data 159
7.3 Neutrino oscillations 162
7.3.1 Matter effects 164
7.3.2 Oscillation parameters 165

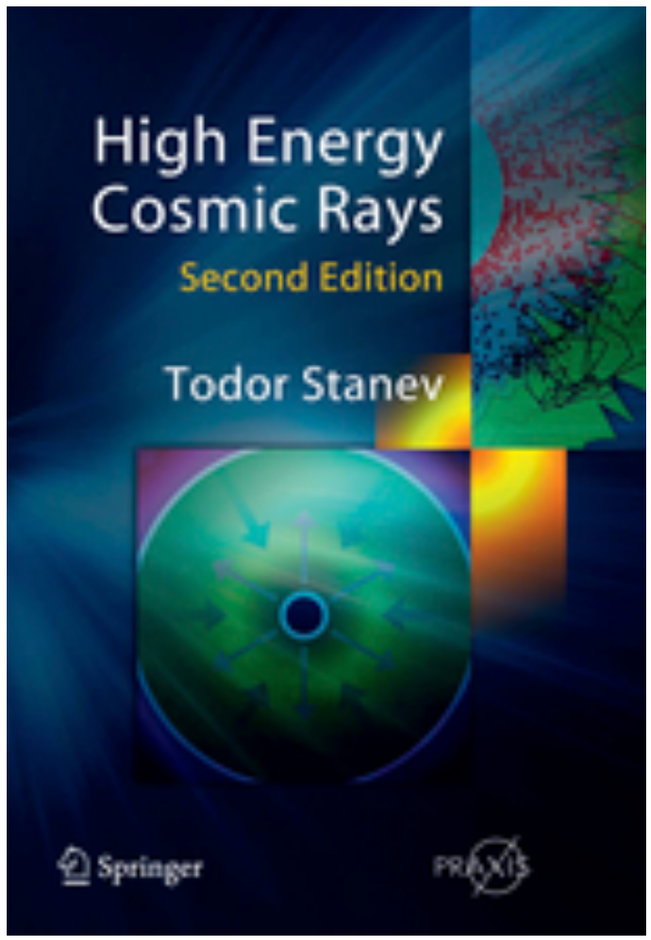

Atmospheric neutrinos

GeV neutrinos originate in pion decay chain $\pi^+ \rightarrow \mu^+ + \nu_\mu; \mu^+ \rightarrow e^+ + \nu_e + \bar{\nu}_\mu$
(and corresponding reactions for π^-**)**

decay length for 1 GeV muon ~6 km
characteristic length for vertical atmospheric cascade ~20 km

mesons + muons decay
—> spectrum of neutrinos follows spectrum of primary CRs

In addition, the charged pion decay chain generates a muon neutrino/antineutrino pair $\nu_\mu \bar{\nu}_\mu$ for every electron neutrino ν_e or antineutrino $\bar{\nu}_e$. These three neutrinos take each about 1/4 of the pion energy. The ratio of muon to electron neutrinos then is $\frac{\nu_\mu + \bar{\nu}_\mu}{\nu_e + \bar{\nu}_e} = 2$. This rule of thumb is confirmed by precise numerical calculations and is modified only slightly by the contribution of other meson decays. The ratio of muon to electron neutrinos is known much better than the absolute flux of neutrinos. With increasing energy, the secondary pions are more and more likely to interact because of the relativistic increase of their decay length $\gamma c\tau$. Above ϵ_π (= 115 GeV in vertical cascades) kaon decays become a much more important source of neutrinos and dominate the neutrino production by 3:1 at asymptotically high energy.

Atmospheric neutrinos

The interaction/decay competition of the secondary mesons steepens the energy spectrum of the neutrinos originating in meson decays by one power of the energy, i.e. if the primary cosmic ray spectrum is $N(E) = A \times E^{-\alpha}$ the spectrum of the meson decay neutrinos is proportional to $E_\nu^{-(\alpha+1)}$. Gaisser [6] calculates the neutrino flux from pion and kaon decay using the decay probability for the mesons and the decay kinematics in the same ways as in (6.11). The result for neutrinos can be expressed as

$$\frac{dN_\nu}{dE_\nu} \simeq 0.0096 E_\nu^{-2.7} \left[\frac{1}{1 + \frac{3.7 E_\nu \cos\theta}{115\ \mathrm{GeV}}} + \frac{0.38}{1 + \frac{1.7 E_\nu \cos\theta}{850\ \mathrm{GeV}}} \right] . \qquad (7.13)$$

Because of the difference in the decay kinematics the contribution of kaons is higher than for muons. Combined with the increasing importance of the second term of (7.13) at high energy this makes kaons asymptotically the major contributor to the muon neutrino flux.

Atmospheric neutrinos

Another power of the energy is added for neutrinos originating in muon decays, which steepens their spectrum to $E_\nu^{-(\alpha+2)}$. For that reason the spectrum of electron neutrinos, that come mostly from muon decays, is steeper than that of muon neutrinos, which are also generated directly in meson decays. At very high energies, when the atmosphere is too thin for muons to decay, neutral kaon decays are the only source of electron neutrinos through the the decay branch $K_L^0 \to \pi^\pm e^\mp \bar{\nu}_e(\nu_e)$.

The ratio of muon to electron neutrinos at high energy depends strongly on the π/K ratio in multiparticle production interactions, which is known only with an accuracy of about 30%. This uncertainty also affects the absolute normalization of the atmospheric neutrino flux. The major factor in the absolute normalization of the atmospheric neutrinos is however the magnitude of the galactic cosmic ray flux interacting in the atmosphere.

Atmospheric neutrinos

The Earth is totally transparent to neutrinos until their mean interaction length $\lambda_\nu = (N_A \sigma_{\nu N})^{-1}$ reaches 10^{10} g/cm^2 – the column density through the center of the Earth. This happens for neutrino energies about 10^5 GeV and does not affect the detection of atmospheric neutrinos because by that energy the atmospheric neutrino flux has decreased by many orders of magnitude. A neutrino detector thus can detect neutrinos in 4π solid angle. Neutrinos coming from below are produced in the atmosphere of the opposite hemisphere. A major feature of the atmospheric neutrino flux is its isotropy. In the absence of geomagnetic cutoffs the neutrino flux underground would be the same from above and from below as shown in Fig. 7.5. The r^{-2} effect from the distance to the production layer of atmosphere is compensated exactly by the larger fraction of the atmosphere seen in any solid angle.

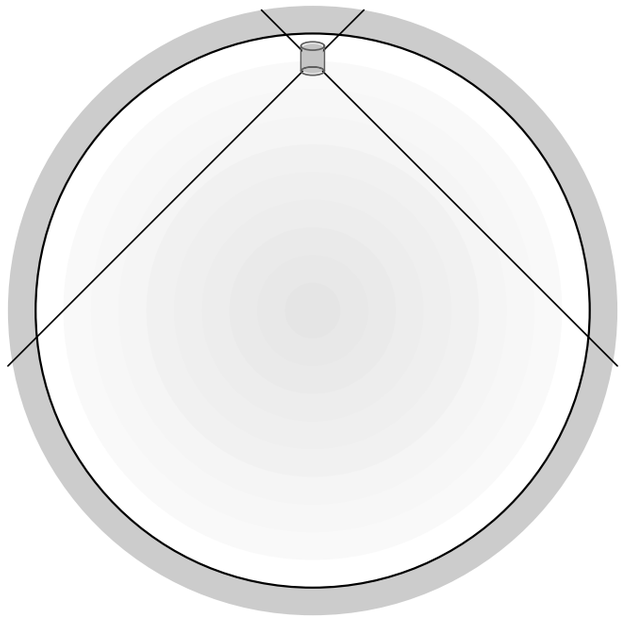

Fig. 7.5. Isotropy of the atmospheric neutrino flux underground in the absence of geomagnetic cutoffs. The detector is much closer to the atmosphere above it but sees a much larger fraction of the atmosphere below it. The flux of downward-going and upward-going neutrinos is the same.

Neutrino detection

Neutrinos are detected mostly through their charged current interaction $\nu_i + N \Rightarrow \ell_i + X$ where the lepton number i is transferred to the corresponding lepton. What experiments see is an electron or muon track originating inside the detector. Assuming that the atmospheric neutrino flux is of the order of 1 $\mathrm{cm}^{-2}\,\mathrm{s}^{-1}$ and the neutrino cross-section is of the order of $10^{-38}\,\mathrm{cm}^2$ one can estimate the necessary detector size. The event rate is

$$
\begin{aligned}
&F_\nu \times \sigma_\nu \times N_A \\
&\quad = 1 \times 10^{-38} \times 6.10^{23} = 6.10^{-15} \text{ per gram per second} \\
&\quad = 1.8 \times 10^{-7} \text{ per gram per year} \\
&\quad = 180 \text{ per 1,000 tons (Kt) per year}
\end{aligned}
$$

Detectors have to have sizes of thousands of tons and to operate for years to collect reasonable atmospheric neutrino statistics. They have to be shielded from downward-going atmospheric muons, which places them deep underground. A large fraction of the total volume of the detector (close to the walls) is not used in neutrino detection because it is often polluted by natural radioactivity. It is used as anti-coincidence counter to reject entering tracks. The inner part of the detector is its fiducial volume.

Neutrino detection

There are two types of detectors:

- traditional calorimeters, where layers of particle detectors are interspaced by layers of target material, e.g. iron.
- water-Cherenkov detectors: photo tubes on the walls of a large tank filled with water detect Cherenkov radiation from the charged particles created in the neutrino–nucleon interaction.

Each detector type has its advantages: Cherenkov detectors are cheaper and can reach total volumes of tens of Kt. Particle calorimeters can measure the charged particle tracks more precisely.

calorimeter

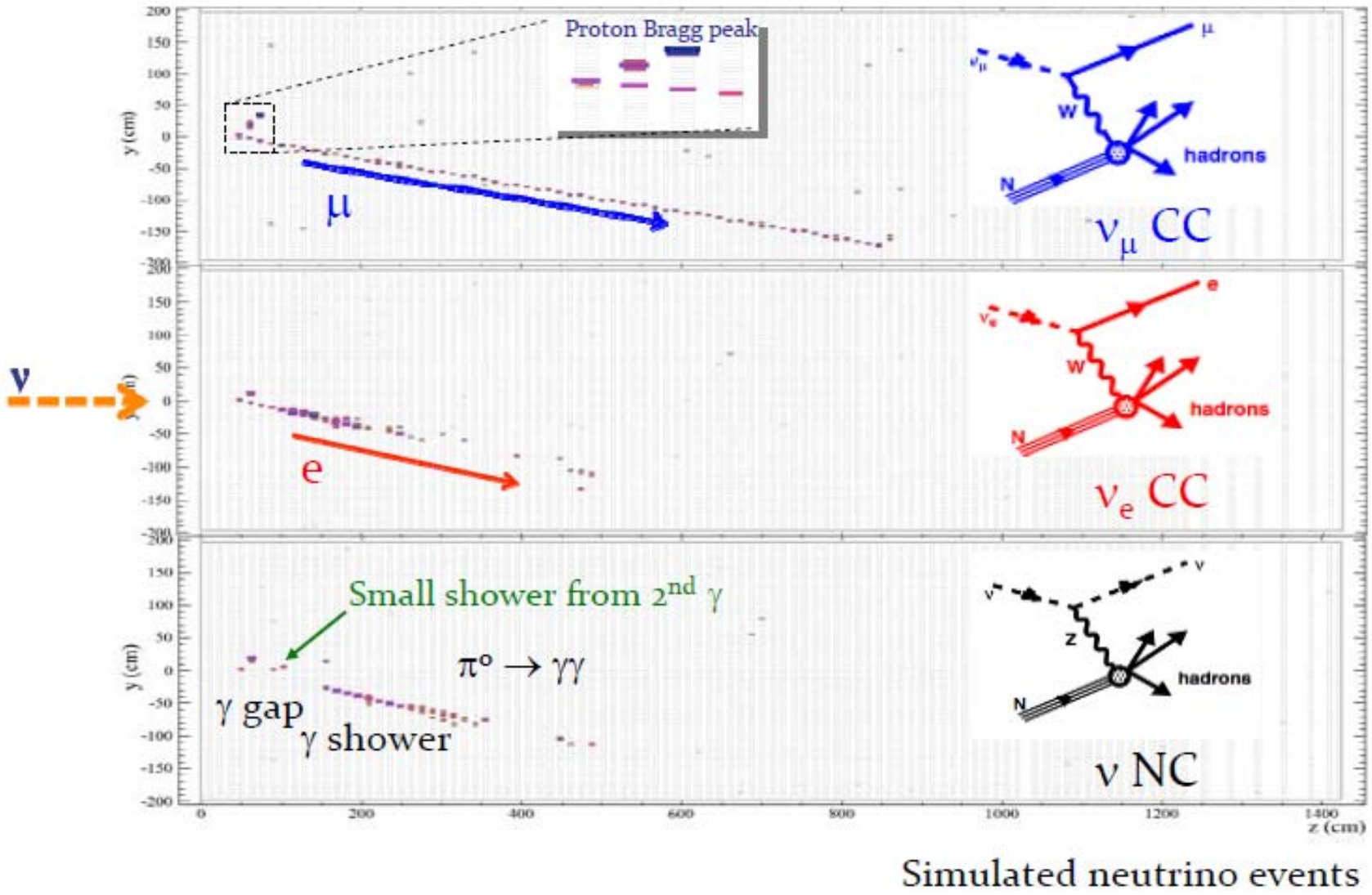

Figure 4. Neutrino interaction processes in the NOνA detectors; (top) a ν_μ charged current event with long muon track and a recoil proton, (middle) a ν_e charged current event with a typical electron shower, and (bottom) a ν neutral current event with a π^0 in the final state.

Super-Kamiokande water Cherenkov detector

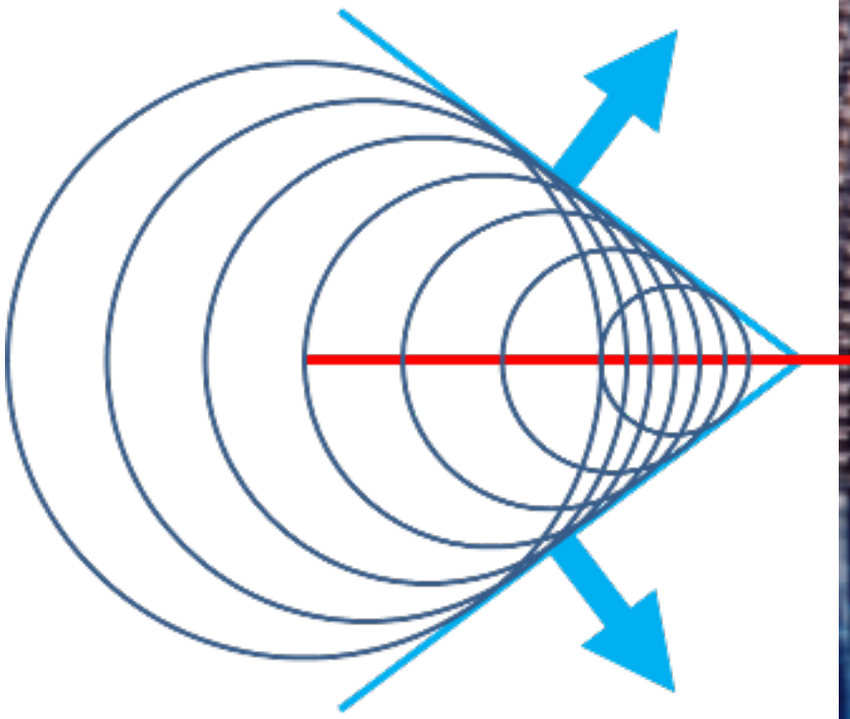

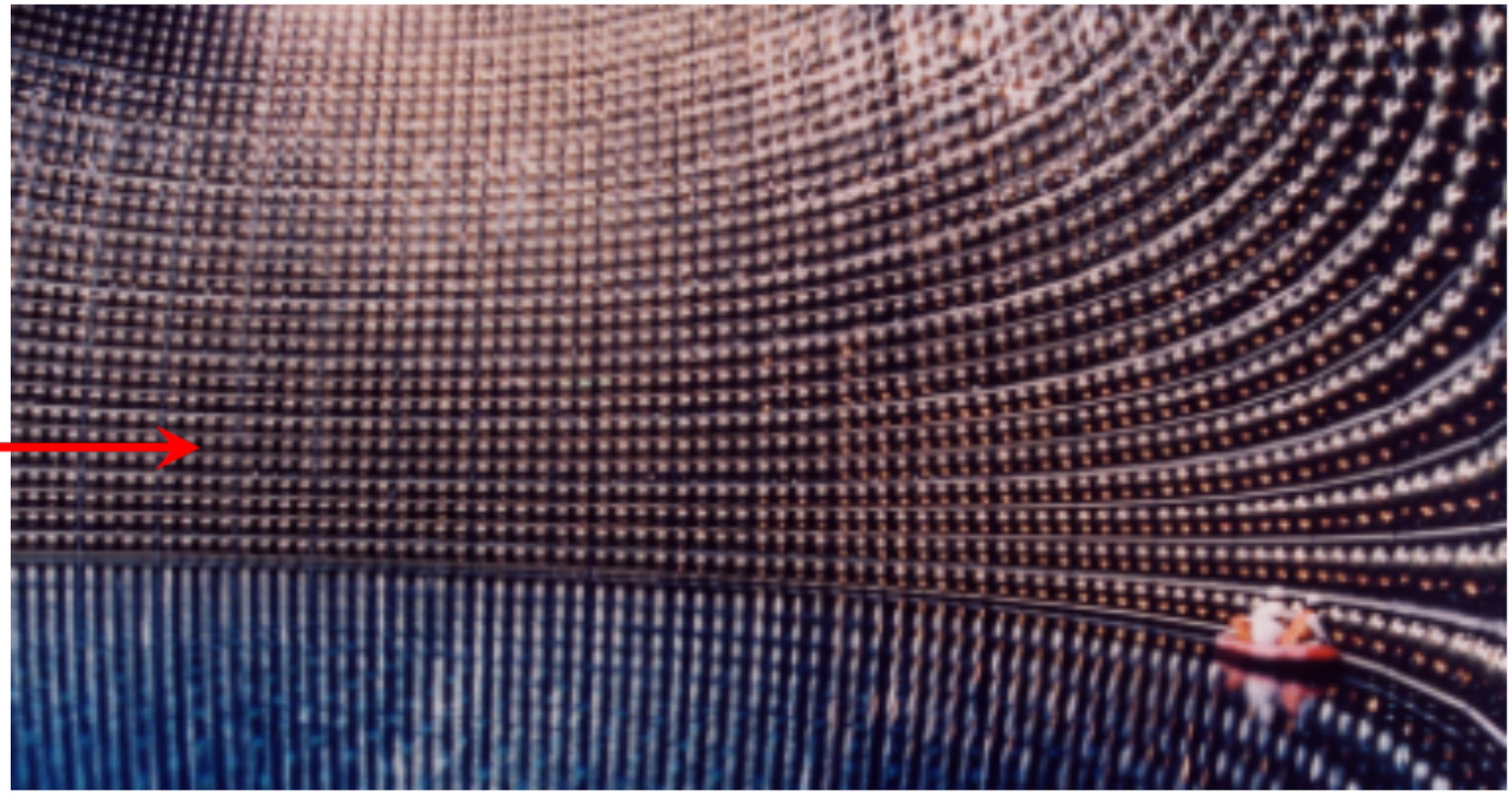

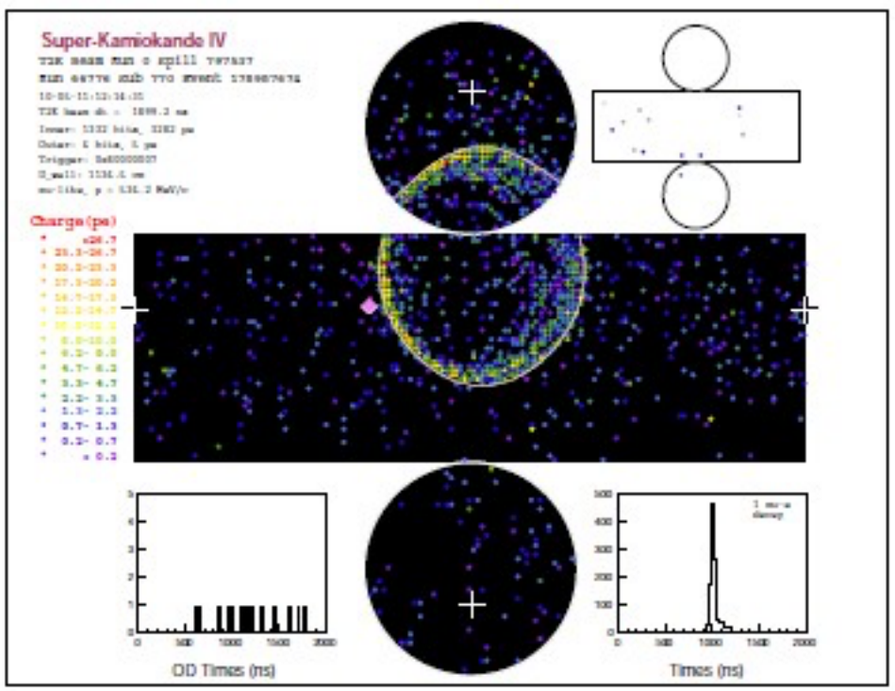

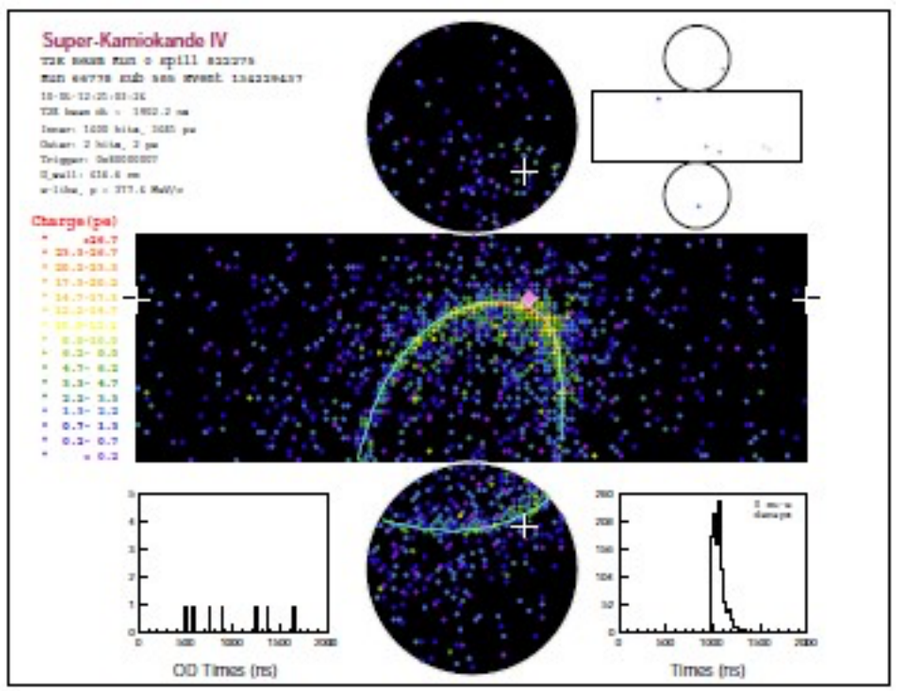

Neutrino detection

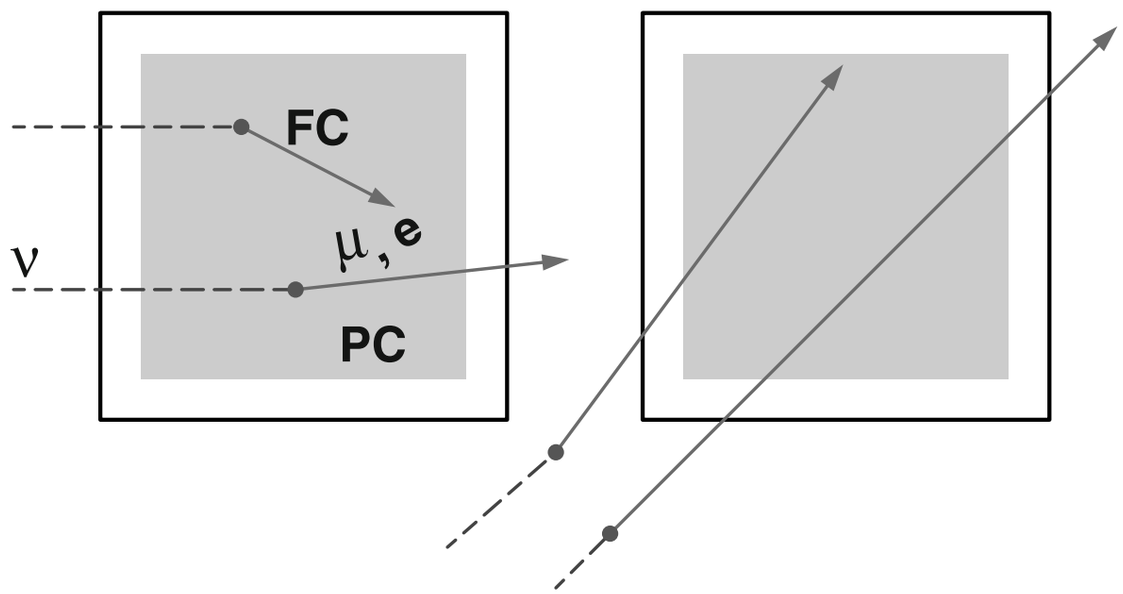

Fig. 7.6. The shaded area represents the fiducial volume of the detector. The left-hand panel shows the geometry of the fully (FC) and partially (PC) contained events. The right-hand figure shows through-going (below) and stopping neutrino-induced muons.

Experimentally neutrino events are classified generally in three groups, which are shown schematically in Fig. 7.6:

- Fully contained (FC) events for which the interaction vertex and all tracks are fully contained in the fiducial volume of the detector. Both the direction and the energy of the daughter leptons can be measured. 4π
- Partially contained (PC) events where only the interaction vertex is contained. Only the direction can be measured and a minimum energy of the lepton can be assigned. PC events are almost exclusively muons. 4π
- Upward-going muons, which are generated by neutrino interactions in the rock surrounding the detector. Upward-going muons can be through-going (exit the detector) or stopping inside the detector. The direction is known but the energy of the muon at production is not. 2π

Neutrino detection

Each type of experimental neutrino event is generated by an energy range of atmospheric neutrinos. The exact distribution depends on the experimental details and on the location of the experiment. Figure 7.7 shows the energy distribution of muon neutrinos responsible for the different event types in the Super-Kamiokande detector. FC events are generated by neutrinos of average energy about 1 GeV. The neutrino energy response for PC events and stopping upward going-muons peaks at 3–5 GeV and through-going upward muons are produced by neutrinos in a wide energy range that peaks at about 100 GeV. Other detectors have slightly different energy responses, but the energy ranges are roughly the same.

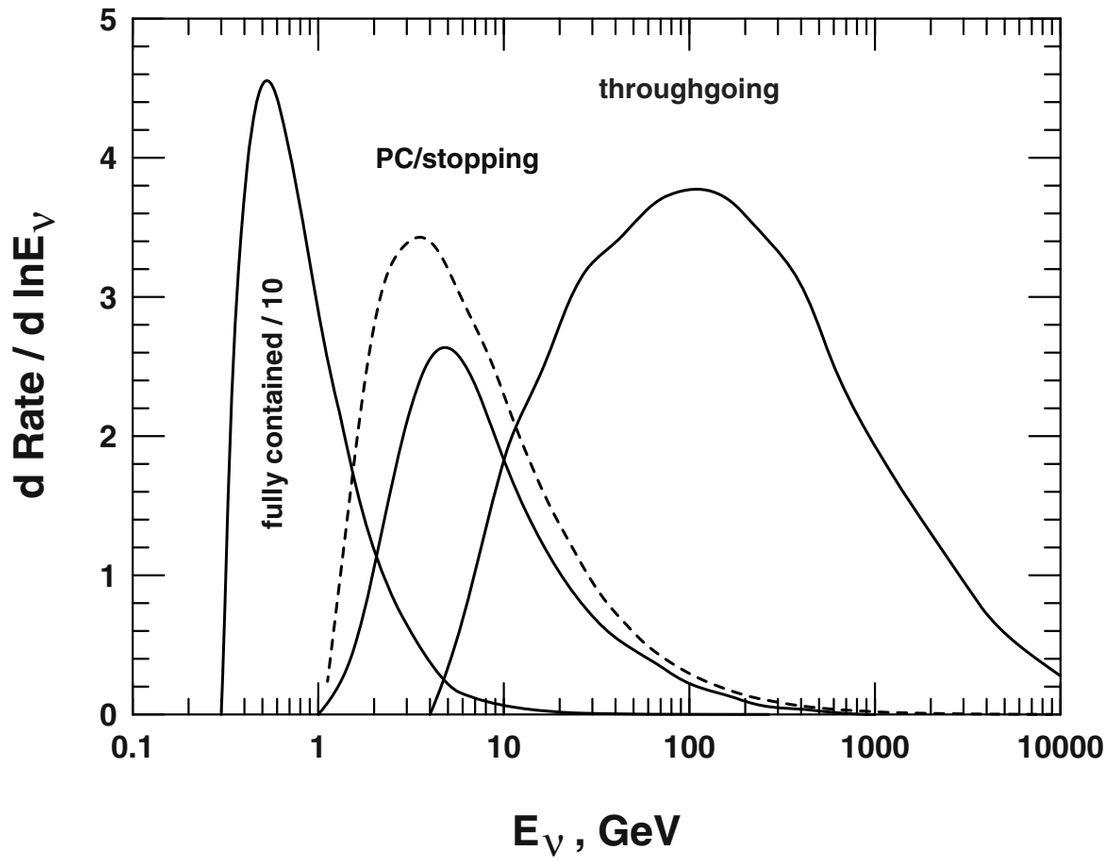

Fig. 7.7. Energy distribution of neutrinos responsible for different types of experimental events. The curves are labeled and the one for PC events is plotted with a dashed line. Note that the curve for fully contained events is scaled down by a factor of 10. The units for the rate are $(\mathrm{Kt.yr})^{-1}$.

Neutrino detection

The rate of contained neutrino events (FC or CC) is calculated by an integration over the neutrino spectrum and the probability that a neutrino of energy E_ν can generate a lepton of energy E_l. For leptons of energy between E_1 and E_2 the rate is

$$\text{Rate} \;=\; N_A \int_{E_1}^{E_2} dE_l \int_{E_l}^{E_\nu - m_l} \frac{dN}{dE_\nu} \left(\frac{d\sigma(E_\nu)}{dy} \right)_{y=1-E_l/E_\nu} dE_\nu \;, \tag{7.14}$$

where σ is the neutrino interaction cross-section, m_l is the mass of the lepton, and $y = 1 - E_l/E_\nu$ is the Bjorken variable. The rate for upward-going muons includes the muon range and is discussed in Sect. 7.2.1.

Muon neutrino cross section

deep inelastic scattering

(DIS) [202] $\nu + N \rightarrow l + N + X$, where X could be one or more hadrons

quasi-elastic scattering [201] $\nu(\bar{\nu}) + n(p) \rightarrow l^{\mp} + p(n)$

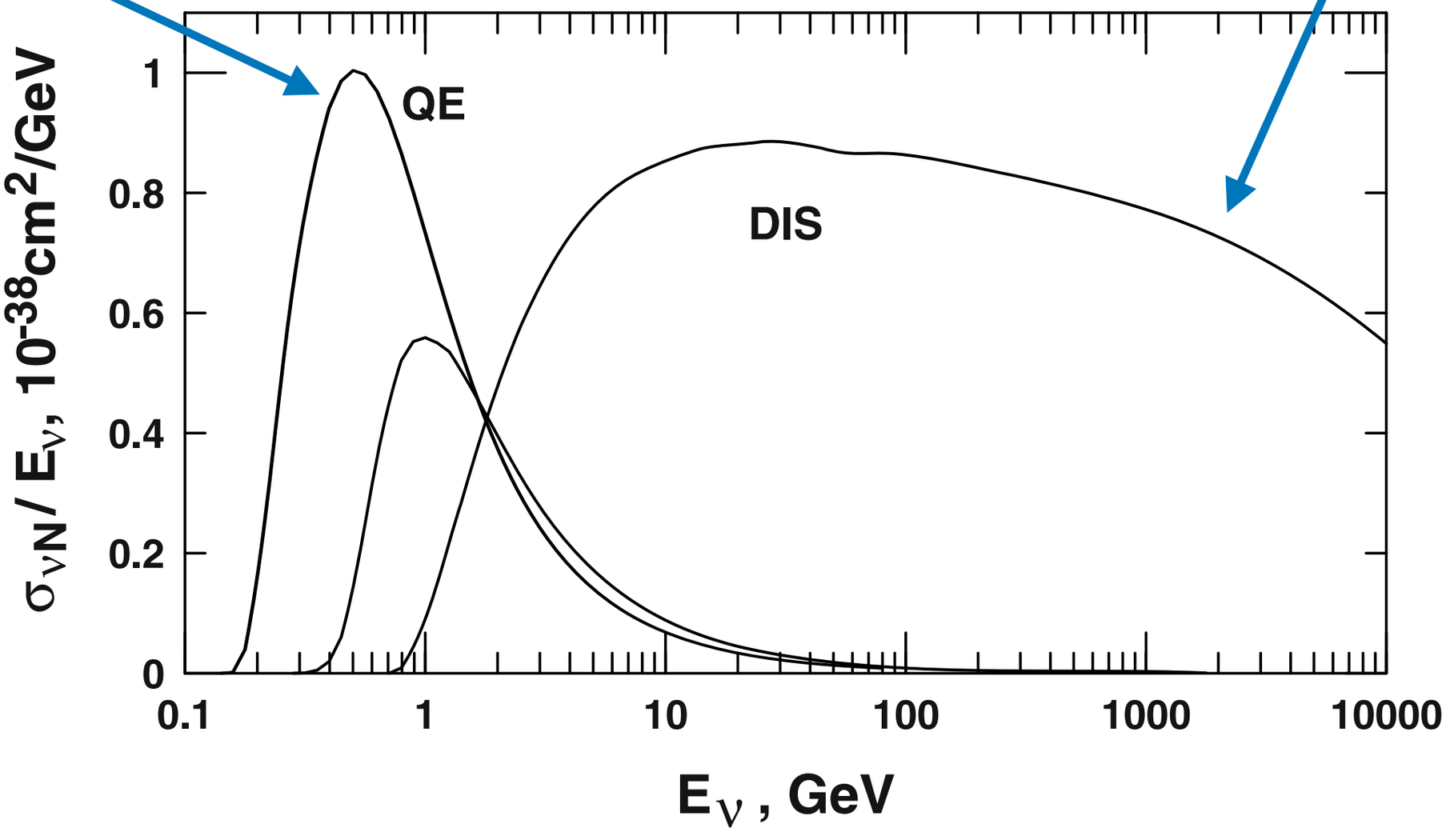

Fig. 7.8. Muon neutrino cross-section as a function of the neutrino energy. QE and DIS cross-sections are labeled. In between is the 1π cross-section.

Upward going muons

Neutrino detection through upward-going muons was developed long ago, because it increases significantly the effective volume of the neutrino detector. Imagine a detector with surface area A, height h and volume $V = h \times A$ as shown in Fig. 7.9. For fully contained events the fiducial volume will be less than one half V. For upward-going muons the effective volume of the detector will be increased R_{eff}/h times which could be a very significant number. For muons of energy 1 TeV $R_{eff} = 2.7$ km.w.e. For a water-Cherenkov detector of height 27 m (taller than a eight-story house) the increase is 100 times. The first detections of atmospheric neutrinos [182, 183] were with neutrino-induced muons.

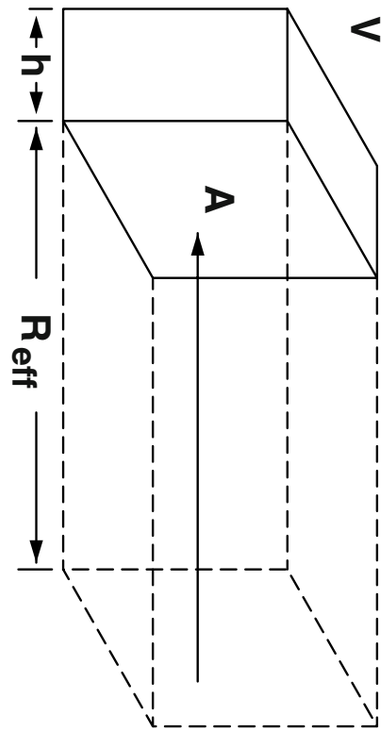

Fig. 7.9. Schematic presentation of the idea for detection of upward-going neutrino-induced muons.

EVIDENCE FOR HIGH-ENERGY COSMIC-RAY NEUTRINO INTERACTIONS*

F. Reines, M. F. Crouch, T. L. Jenkins, W. R. Kropp, H. S. Gurr, and G. R. Smith

Case Institute of Technology, Cleveland, Ohio

and

J. P. F. Sellschop and B. Meyer

University of the Witwatersrand, Johannesburg, Republic of South Africa

(Received 26 July 1965)

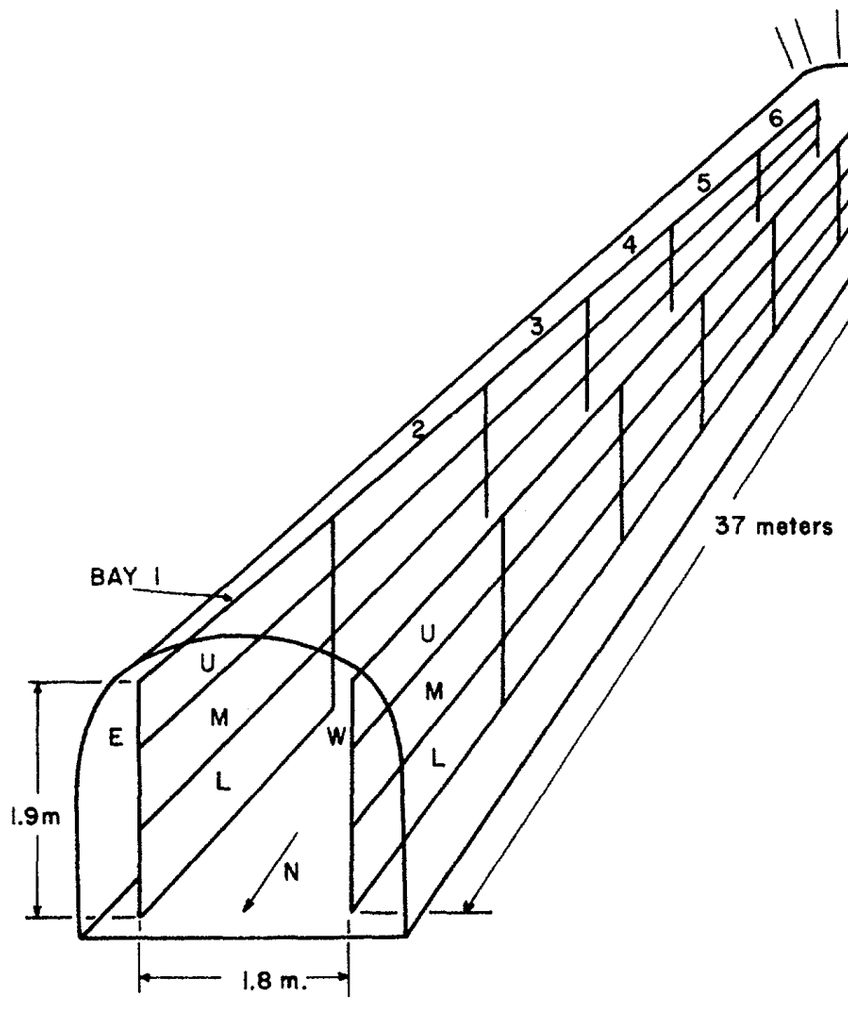

FIG. 1. Schematic of detector array.

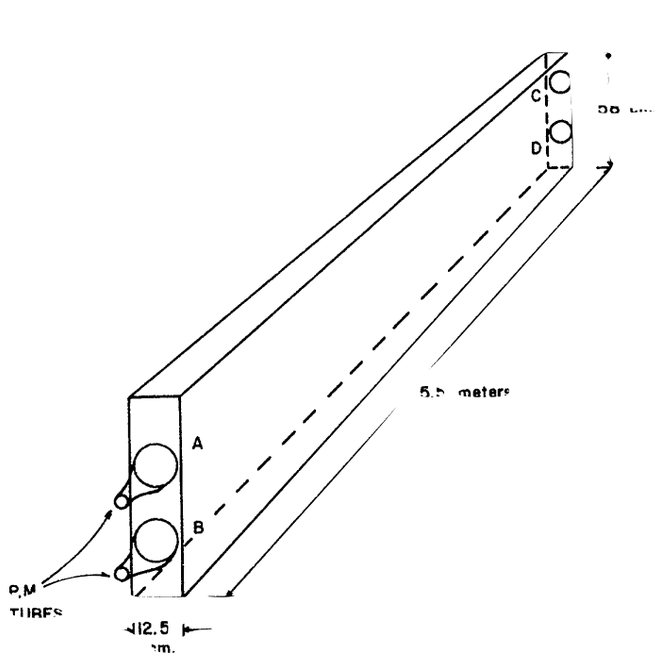

FIG. 2. Sketch of detector element.

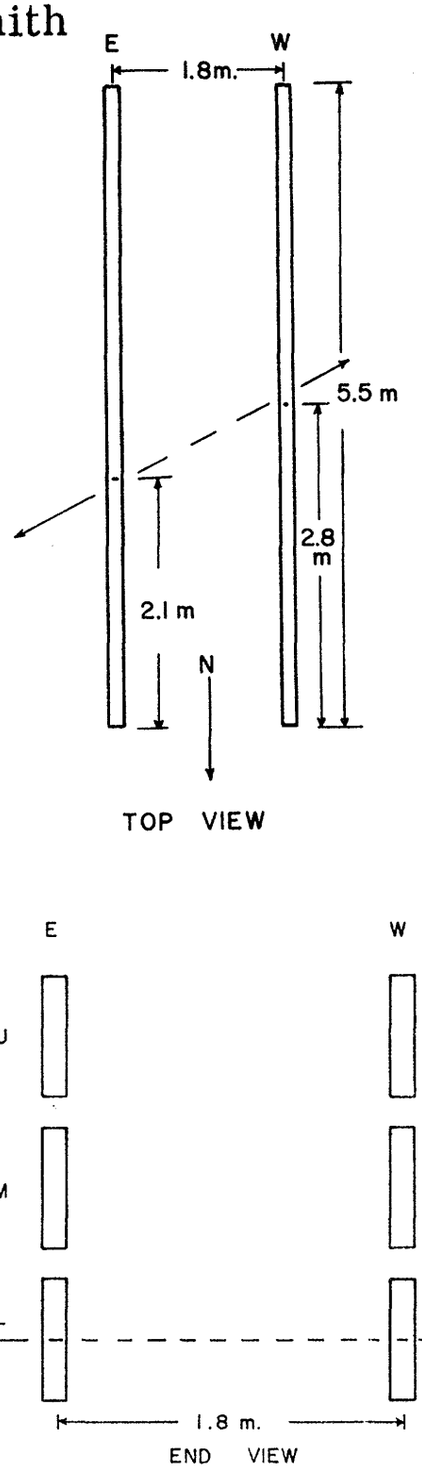

FIG. 3. Reconstruction of event of 23 February 1965

DETECTION OF MUONS PRODUCED BY COSMIC RAY NEUTRINOS DEEP UNDERGROUND

C. V. ACHAR, M. G. K. MENON, V. S. NARASIMHAM, P. V. RAMANA MURTHY and B. V. SREEKANTAN,
Tata Institute of Fundamental Research, Colaba, Bombay

K. HINOTANI and S. MIYAKE,
Osaka City University, Osaka, Japan

D. R. CREED, J. L. OSBORNE, J. B. M. PATTISON and A. W. WOLFENDALE
University of Durham, Durham, U.K.

Received 12 July 1965

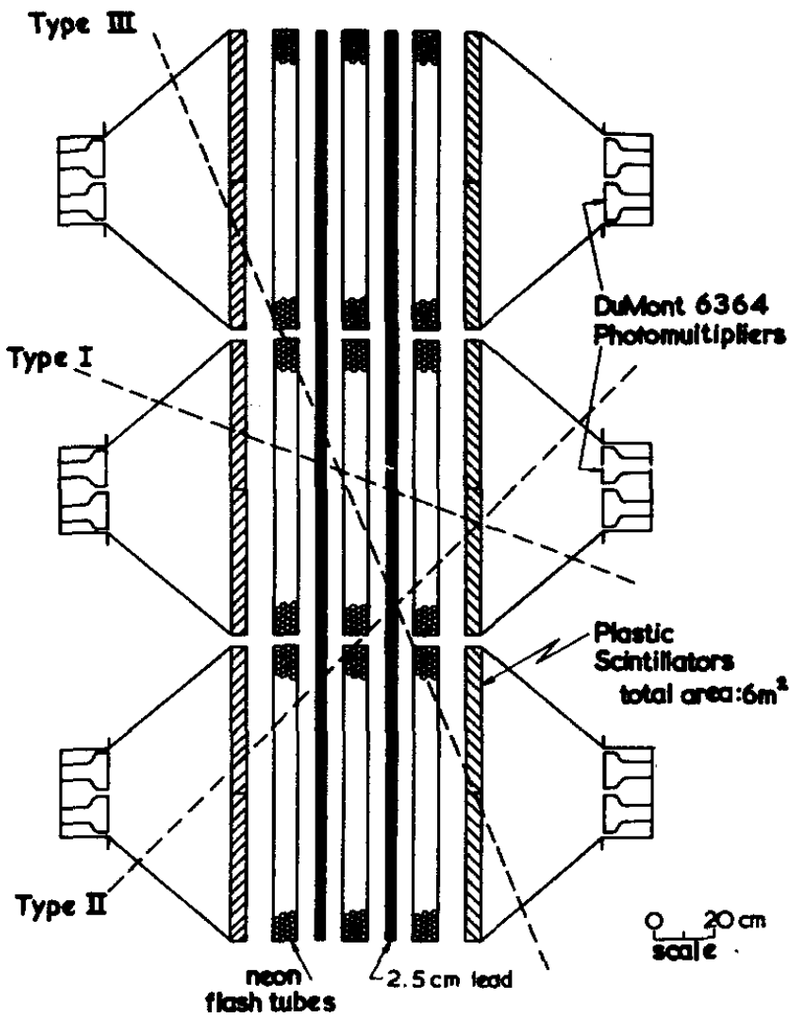

Fig. 1. Neutrino telescope.

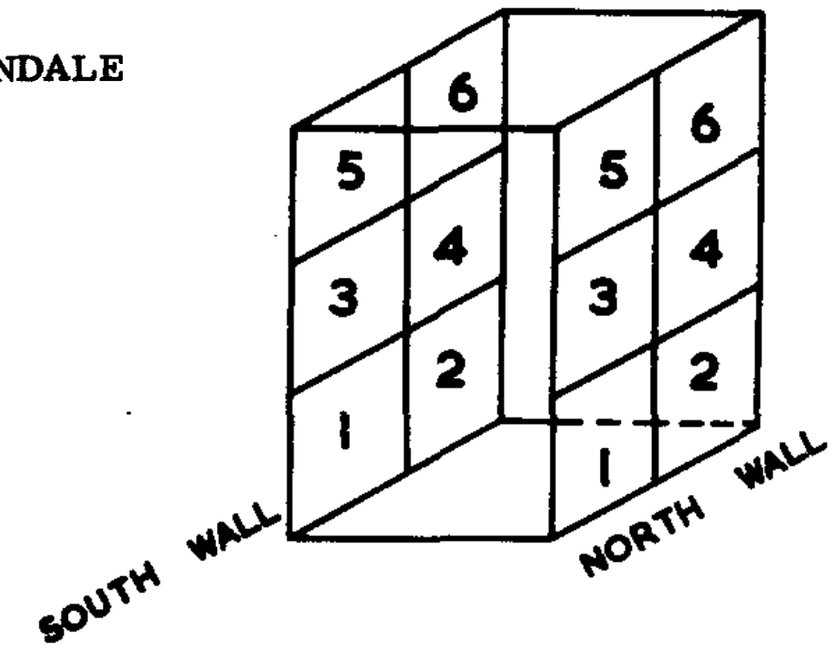

TYPE I EVENTS: $(N_{1OR2} + S_{1OR2})$ OR $(N_{3OR4} + S_{3OR4})$ OR $(N_{5OR6} + S_{5OR6})$

TYPE II EVENTS: $(N_{3OR4} + S_{1OR2})$ OR $(N_{3OR4} + S_{5OR6})$ OR $(N_{5OR6} + S_{3OR4})$ OR $(N_{1OR2} + S_{3OR4})$

TYPE III EVENTS $(N_{1OR2} + S_{5OR6})$ OR $(N_{5OR6} + S_{1OR2})$

N MEANS NORTH: S MEANS SOUTH

Fig. 2.

coincidences are recorded between a pair of photomultipliers on one wall and any pair on the other wall.

Upward going muons

The rate of neutrino-induced upward-going muons is obtained similarly to (7.14) with the evaluation of $d\sigma_{\nu}/dy$ replaced by the probability $P_{\nu\mu}(E_\nu, E_\mu)$ that a neutrino of energy E_ν will produce a muon of energy above E_μ at the detector [198, 199, 200], i.e.

$$\text{Rate}_{\text{up}}(> E_\mu) \;=\; \int_{E_\mu}^{\infty} dE_\mu \int_{E_\mu}^{E_\nu - m_\mu} \frac{dN}{dE_\nu}\, P_{\nu\mu}(E_\nu, E_\mu)\, dE_\mu \tag{7.15}$$

The probability $P_{\nu\mu}(E_\nu, E_\mu)$ is given by an integral over the differential neutrino cross-section $d\sigma/dy$ evaluated at $y = 1 - E'_\mu/E_\nu$ folded with the effective range $R_{eff}(E'_\mu, E_\mu)$ of a muon of energy E'_μ to reach the detector with energy E_μ.

$$P_{\nu\mu}(E_\nu, E_\mu) \;=\; N_A \int_0^{E_\nu} dE'_\mu \left(\frac{d\sigma(E_\nu)}{dy}\right)_{y=1-E'_\mu/E_\nu} R_{eff}(E'_\mu, E_\mu) \tag{7.16}$$

Upward going muons

Figure 7.10 gives the probability $P_{\nu\mu}$ for muon energy of 1 GeV and of 1 TeV. The expectations for the vertical (lower line) and horizontal (upper line) flux of neutrino-induced muons of energy above 1 GeV are plotted in Fig. 7.1.

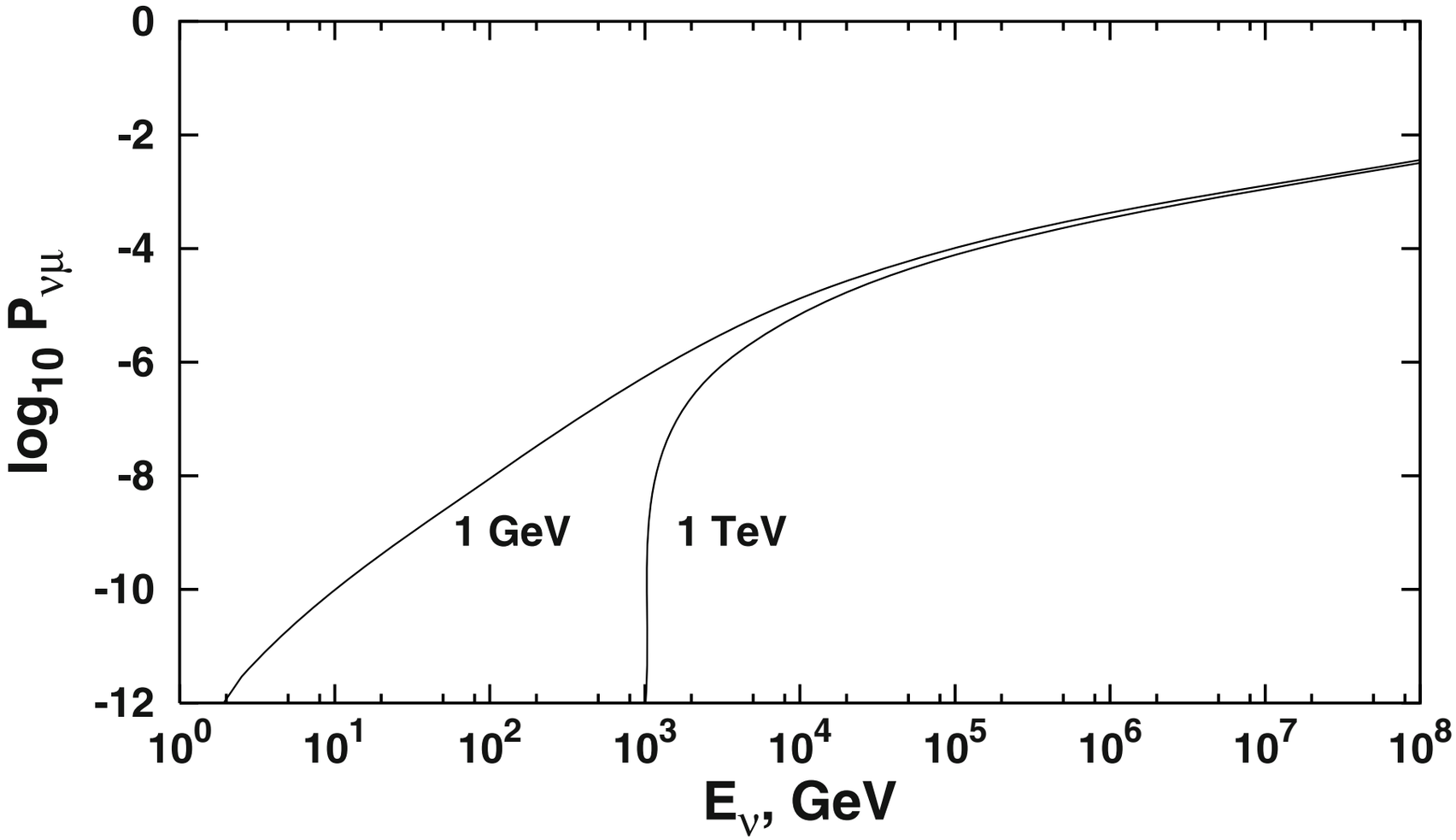

Fig. 7.10. Probability that a neutrino of energy E_ν will produce a muon of energy 1 GeV and 1 TeV at the detector in standard rock.

Neutrino flux calculations

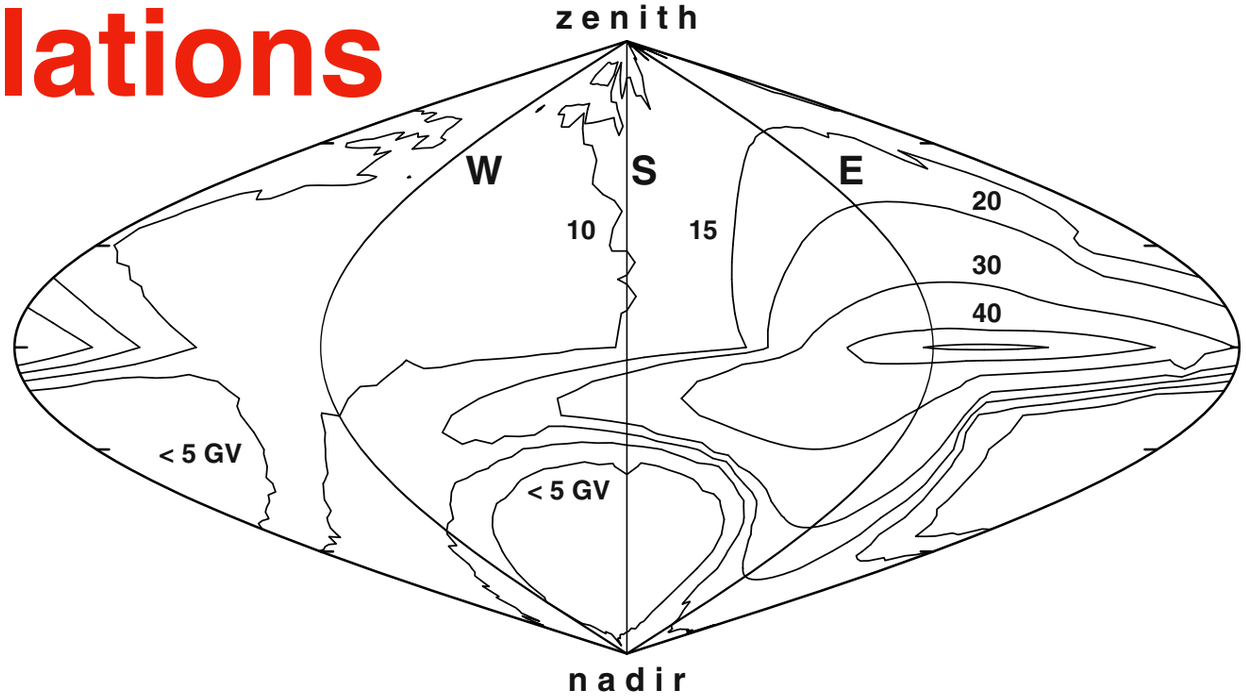

Fig. 7.11. Contour map of the geomagnetic cutoff at Kamioka. Contours connect the directions with equal rigidity cutoffs. East, south and west are indicated and north is split at the edge of the graph.

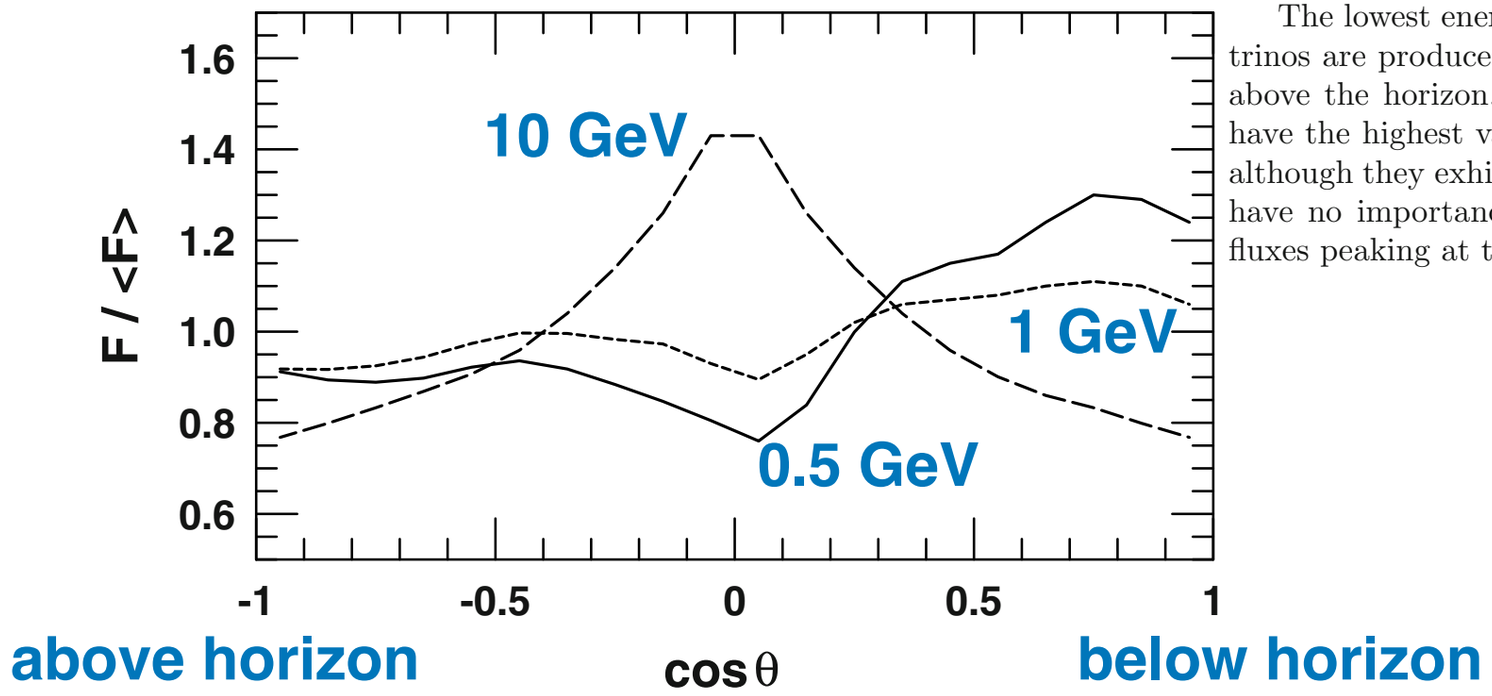

Fig. 7.12. Normalized flux of neutrinos of energy 0.5 (solid line), 1 (dotted line) and 10 GeV (dashed line) at the location of Kamioka as a function of the zenith angle.

The lowest energy neutrinos show the large up/down ratio, i.e. more neutrinos are produced in the hemisphere below the horizon than are produced above the horizon. There is a dip in horizontal direction where the cutoffs have the highest values. Up and down fluxes at 1 GeV are more symmetric, although they exhibit the same structure. The geomagnetic cutoffs at 10 GeV have no importance and one can see the perfectly symmetric picture with fluxes peaking at the horizon.

Neutrino flux calculations

For the same reasons one expects more low energy neutrinos at high geomagnetic latitudes. If the fluxes of upward-going neutrinos at the two locations are about equal, at high geomagnetic latitude the flux of down-going neutrinos will be higher than at low latitudes. Figure 7.13 shows a comparison of the angle-averaged muon neutrino and antineutrino fluxes predicted for locations in Canada and for Kamioka.

To give a more realistic impression of the expectation in event rate the quantity plotted is $E_\nu^2(dN\nu/dE_\nu + \frac{1}{3}dN_{\bar{\nu}}/dE_\nu)$. The $\frac{1}{3}$ factor accounts roughly for the difference between the neutrino and antineutrino cross-sections. One of the E_ν powers accounts, also very roughly, for the energy dependence of the cross-sections.

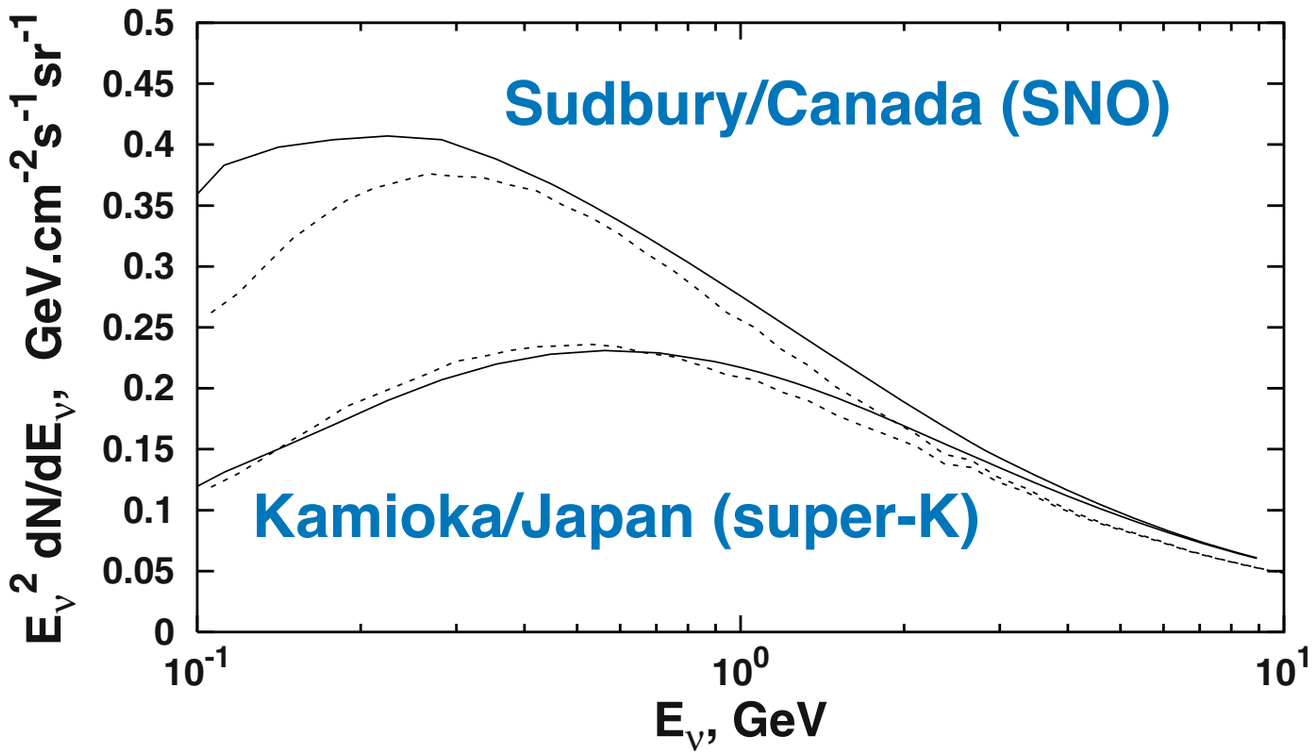

Fig. 7.13. Comparison of the fluxes of $\nu_\mu + \bar{\nu}_\mu$ for the locations of Sudbury and Kamioka. Solid lines are from Ref. [179] and the dashed lines from Ref. [210].

Super Kamiokande

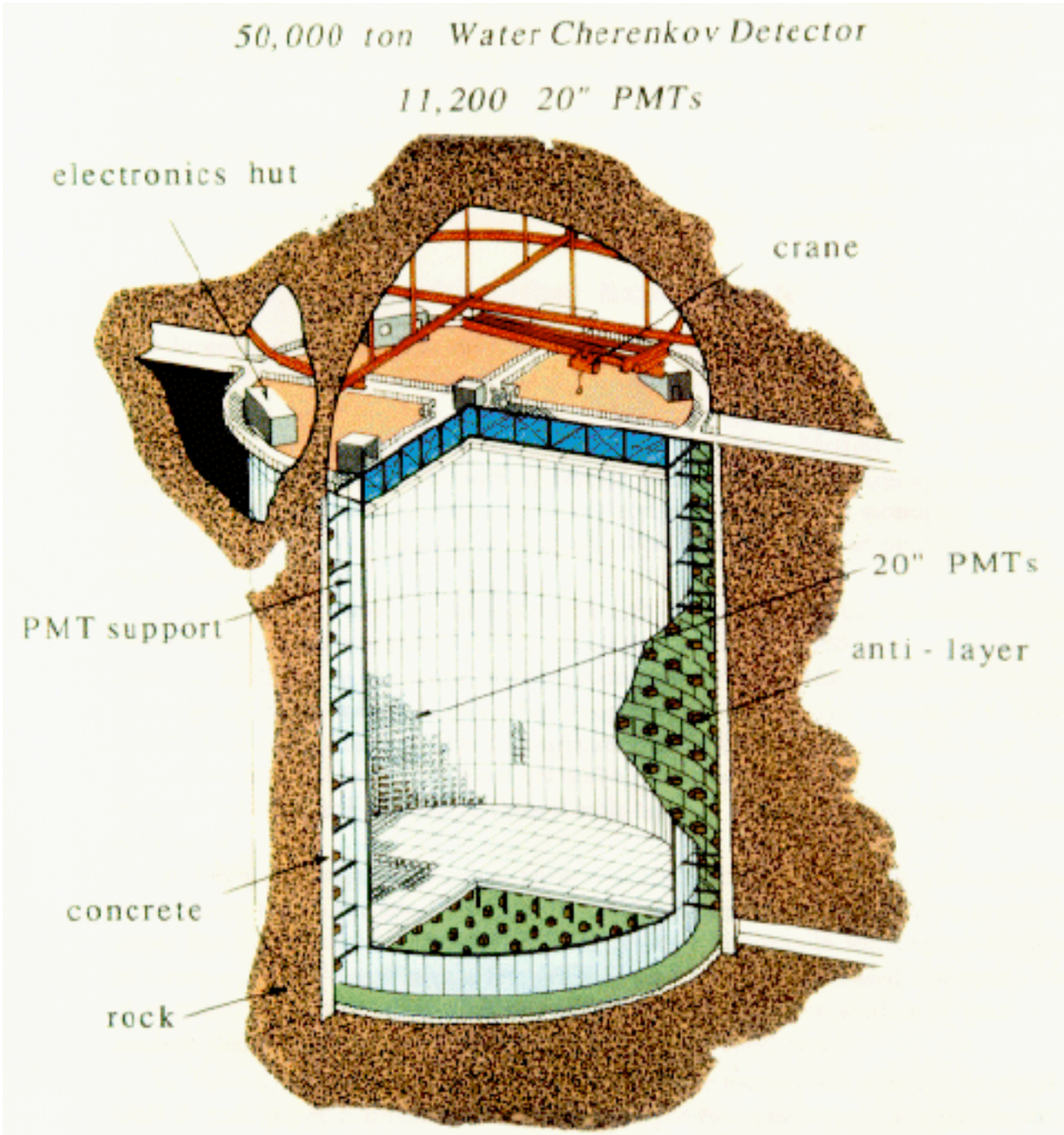

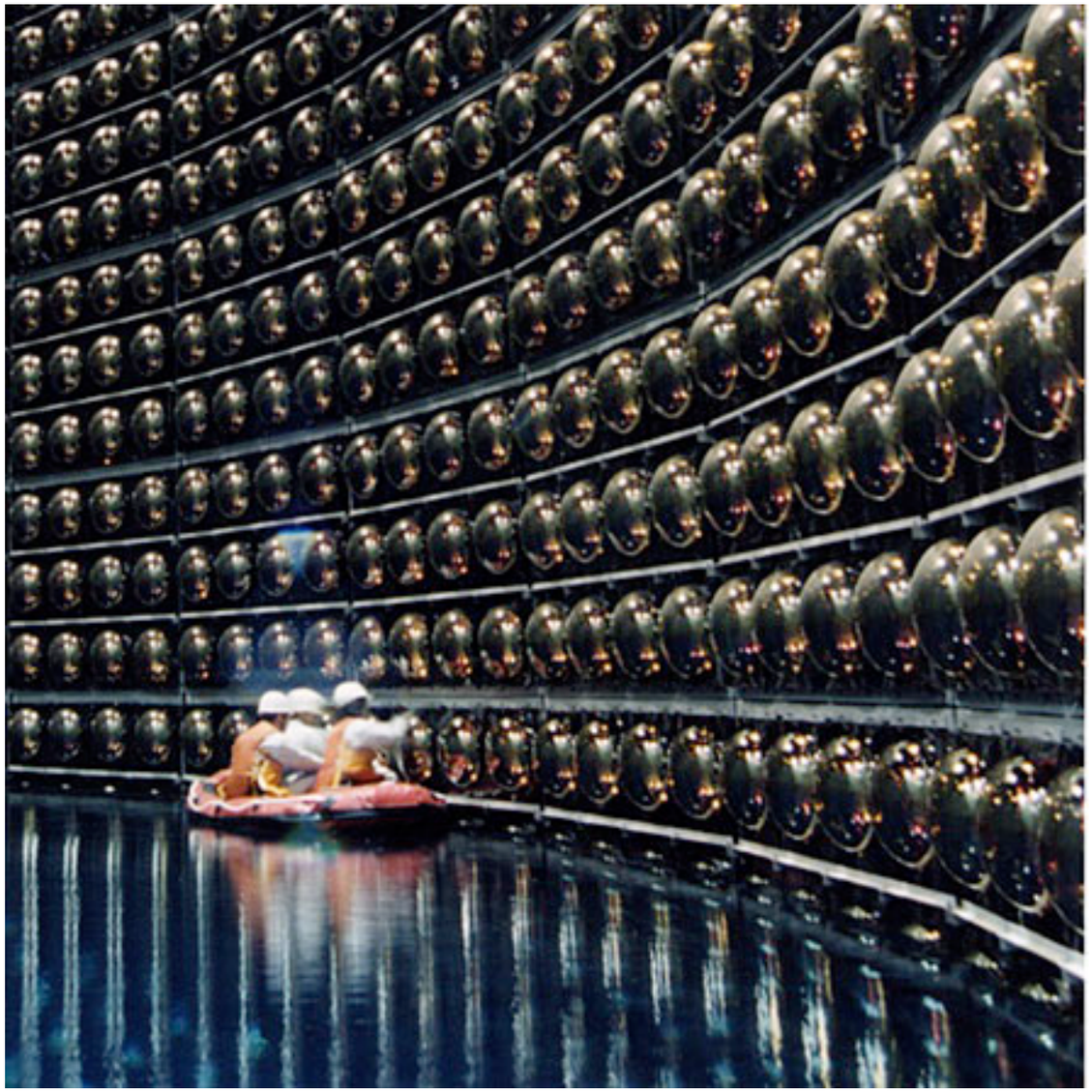

neutrinos are also produced in air showers

--> atmospheric neutrinos

$$p + N \rightarrow \pi^{\pm} + X$$

CR **air**

$$\pi^{\pm} \rightarrow \mu^{\pm} + \overset{(-)}{\nu}_{\mu}$$

$$\mu^{\pm} \rightarrow e^{\pm} + \overset{(-)}{\nu}_{e} + \overset{(-)}{\nu}_{\mu}$$

expect $1\nu_e \quad 2\nu_\mu$

ratio $R = \dfrac{\nu_\mu + \bar{\nu}_\mu}{\nu_e + \bar{\nu}_e} = 2$

energies are ~GeV range

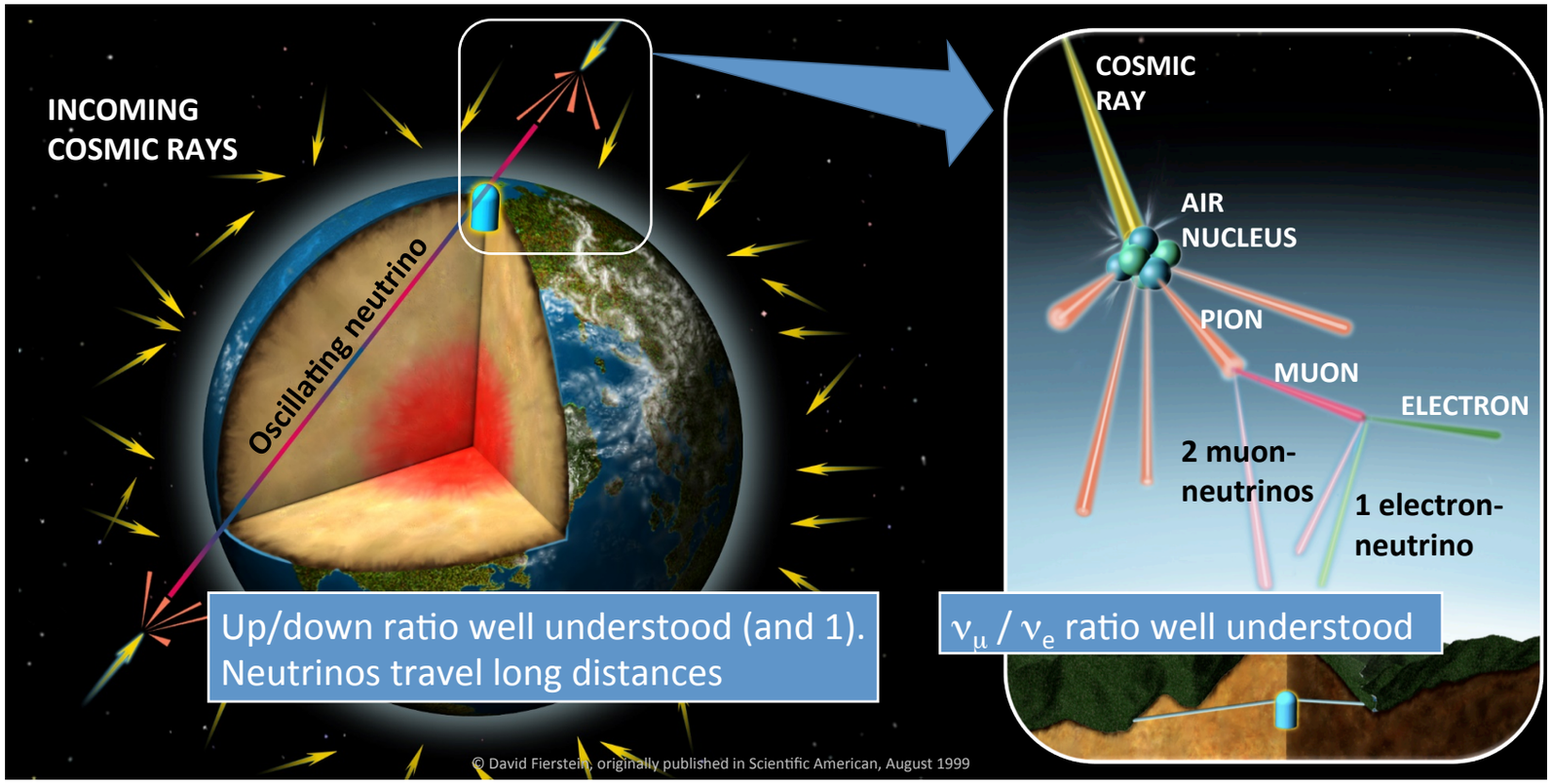

Super Kamiokande

The first clear hint for neutrino oscillations

atmospheric neutrinos

measure ν_e, ν_μ via charged current interactions

$$\begin{cases} \nu_e + A \rightarrow e^- + X \\ \bar{\nu}_e + A \rightarrow e^+ + X \end{cases}$$

$$\begin{cases} \nu_\mu + A \rightarrow \mu^- + X \\ \bar{\nu}_\mu + A \rightarrow \mu^+ + X \end{cases}$$

$e^\pm$ and $\mu^\pm$ are detected via Cherenkov light in water

Neutrino flux measurements

The spectrum of Fig. 7.15 cannot be directly compared with the predictions for the neutrino fluxes. To start with, only a fraction of the neutrino energy is transferred to the leptons. This fraction varies on an event by event basis and is different for QE, 1π and DIS interactions. In addition there are detector biases that are different for muons and electrons. Muons are heavier and respectively have higher threshold for emission of Cherenkov light. Electrons lose their energy faster and are contained more easily in the detector as FC events. High energy muons leave the detector, become PC events and their energy cannot be determined. Finally there is some ambiguity in the determination the type of the lepton in a water-Cherenkov detector. Remember that this is done by the shape of the signal which is on the average different – muons produce a cleaner circle on the wall of the detector than electrons.

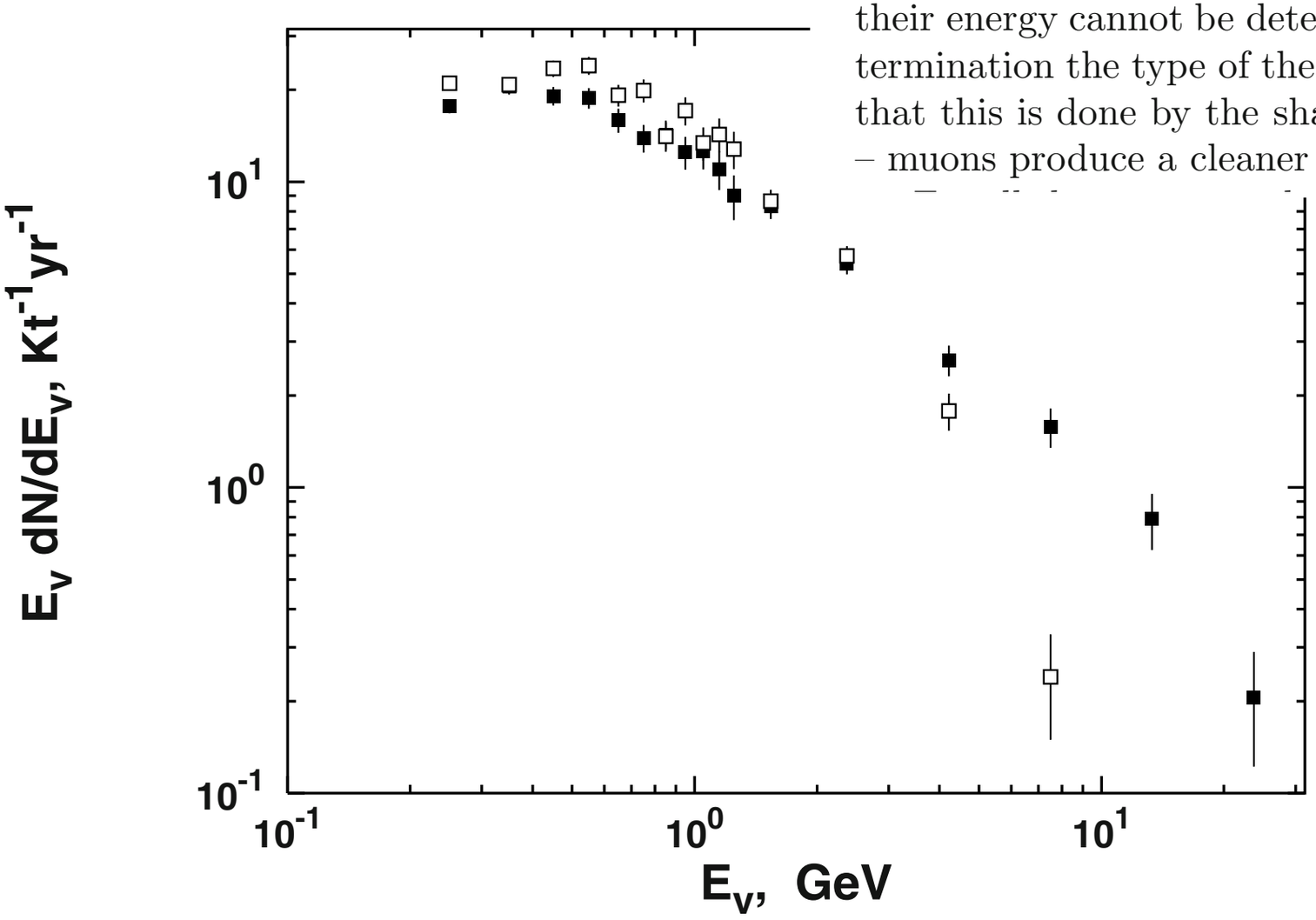

Fig. 7.15. Energy spectrum of muon-like (open symbols) and e-like (closed symbols) events detected by Super-K. E_v is the visible energy of the detected leptons.

Deficit of neutrinos

$$R2 = \frac{R(\mu/e)_{\rm observed}}{R(\mu/e)_{\rm predicted}} \sim \frac{1.25}{2.00} \sim 0.6 \qquad (7.22)$$

for the GeV flux of Fig. 7.15. The ratio cannot be deduced by eye from the figure at higher energy as the experimental efficiency for muons strongly decreases. $R2$ is calculated by a comparison with the Monte Carlo predictions.

Table 7.1 compares the results from several different experiments. Note that the Kamiokande and Super-K results are separated in sub-GeV and multi-GeV samples. The division is at $E_\nu = 1.33$ GeV. The results for contained events in Table 7.1 are only for 'single-ring' or 'single-track' events, i.e. when only one lepton above the threshold is generated in the neutrino interactions. The analysis of 'multi-ring' events is much more difficult.

Table 7.1. Experimental data on the double ratio $R2$ in different experiments. The first error is statistical and the second one is systematic. For upward-going muons the values are for the ratio between observed and predicted rates.

Experiment	Kt.yr	double ratio
IMB	7.7	$0.54 \pm 0.05 \pm 0.11$
Frejus	2.0	$1.00 \pm 0.15 \pm 0.08$
Nusex	0.74	0.96 ± 0.30
Soudan2	5.1	$0.68 \pm 0.11 \pm 0.05$
sub-GeV		
Kamiokande	7.7	$0.60 \pm 0.06 \pm 0.05$
Super-K	75.5	$0.66 \pm 0.02 \pm 0.05$
multi-GeV		
Kamiokande	8.2	$0.57 \pm 0.08 \pm 0.07$
Super-K	75.5	$0.68 \pm 0.03 \pm 0.08$
Super-K (PC)	75.5	$0.71 \pm 0.05 \pm 0.08$
upward muons		
Kamiokande	14.4	$0.75 \pm 0.06 \pm 0.05$
Super-K	75.0	$0.92 \pm 0.03 \pm 0.05$
MACRO	—	$0.74 \pm 0.04 \pm 0.05$

Neutrino oscillations

SOVIET PHYSICS JETP VOLUME 26, NUMBER 5 MAY, 1968

NEUTRINO EXPERIMENTS AND THE PROBLEM OF CONSERVATION OF LEPTONIC CHARGE

B. PONTECORVO

Joint Institute for Nuclear Research

Submitted June 9, 1967

Zh. Eksp. Teor. Fiz. 53, 1717–1725 (November, 1967)

The possible violations of leptonic charge conservation, which are compatible with experimental data, are large. This paper analyses various experimental setups which would be capable of detecting such hypothetical violations. It is shown that the most sensitive experiments are the search for the process $\mu \to e + \gamma$ and especially a search for oscillations of the type $\nu \rightleftarrows \bar{\nu}$ and $\nu_e \rightleftarrows \nu_\mu$. A nonvanishing neutrino mass could be related to CP-nonconservation and to an electric (and magnetic) dipole moment of the neutrino. Astronomical implications of the oscillation $\nu \rightleftarrows \bar{\nu}$ are discussed.

INTRODUCTION

DATA on lepton conservation have been obtained by different methods for the el-neutrino (ν_e) and for the mu-neutrino (ν_μ). A review of the theoretical and experimental data can be found in [1] and [2] respectively.

The conclusion that $\nu_e \neq \nu_\mu$ follows from the results of [3], from experiments involving the transition $Cl^{37} \to Ar^{37}$ [4], and particularly from the recent investigations of double beta decay in Ca^{48} [5-7]. The rate of the process $Ca^{48} \to {}_{22}Ti^{48} + e^- + e^-$ turns out to be

eral possibilities, which can be summarized in the following manner in terms of conservation of leptonic charge.

1. There are two different additive leptonic charges, muonic and electronic.

2. There is only one additive leptonic charge, the signs of which are opposite for the μ^- and e^- [10]. There exists only one (four-component) neutrino, the left-handed components of which are associated with the electron, and the right-handed ones belong to the muon [11].

Neutrino oscillations

SOVIET PHYSICS JETP VOLUME 26, NUMBER 5 MAY, 1968

NEUTRINO EXPERIMENTS AND THE PROBLEM OF CONSERVATION OF LEPTONIC CHARGE

B. PONTECORVO

OSCILLATIONS AND ASTRONOMY

If the oscillation length is large (>10 km) it will be impossible to observe the transitions $\nu \rightleftarrows \bar{\nu}$, $\nu_\mu \rightleftarrows \nu_e$ in neutrino beams from reactors or accelera-

967)

ation, which are compatible with experimental data, tal setups which would be capable of detecting such sensitive experiments are the search for the process of the type $\nu \rightleftarrows \bar{\nu}$ and $\nu_e \rightleftarrows \nu_\mu$. A nonvanishing tion and to an electric (and magnetic) dipole moment oscillation $\nu \rightleftarrows \bar{\nu}$ are discussed.

tors. However, significant astrophysical effects might be possible.

From the point of view of detection possibilities, an ideal object is the sun. If the oscillation length is much smaller than the radius of the solar region which effectively produces neutrinos (e.g. one tenth of the solar radius $R_\odot$ or 10^5 km for neutrinos from B^8 [23]) which will give the main contribution to the experiments which are being planned now (cf., e.g., [24]), it will be impossible to detect directly oscillations of the solar neutrinos, owing to a smearing out of the effect. The only effect at the surface of the earth would consist in the fact that the flux of observable solar neutrinos would be half as large as the total flux of solar neutrinos. Unfortunately the weight of the various thermonuclear reactions in the sun, and the central temperature of the sun are insufficiently well known in order to allow a useful comparison of expected and observed solar neutrinos, from the point of view of this article [1].

eral possibilities, which can be summarized in the following manner in terms of conservation of leptonic charge.

1. There are two different additive leptonic charges, muonic and electronic.

2. There is only one additive leptonic charge, the signs of which are opposite for the μ^- and e^- [10]. There exists only one (four-component) neutrino, the left-handed components of which are associated with the electron, and the right-handed ones belong to the muon [11].

Neutrino oscillations

Neutrino oscillations were first suggested as a possibility by Pontecorvo [224]. Oscillations imply that neutrinos have nonzero mass. The known neutrino flavor eigenstates can be represented as a linear combination of different 'basic' neutrino flavors. In the simple two-neutrino case this assumption can be expressed as:

$$\begin{aligned} \nu_\alpha &= \cos\theta \times \nu_1 + \sin\theta \times \nu_2 \\ \nu_\beta &= -\sin\theta \times \nu_1 + \cos\theta \times \nu_2 \ , \end{aligned} \tag{7.23}$$

where θ is the mixing angle between ν_1 and ν_2. A calculation of the wave functions for neutrino flavors α and β shows the development of a phase difference $\Delta\phi = \Delta m^2 t/(2E_\nu)$, where $\Delta m^2 = |m_\alpha^2 - m_\beta^2|$ is the absolute value of the difference in the squared masses of the two flavors. This phase difference defines the conversion (oscillation) probability of ν_α into ν_β

$$P_{\nu_\alpha \to \nu_\beta} = \sin^2(2\theta)\sin^2\left(\pi\frac{L}{L_{osc}}\right) \ , \tag{7.24}$$

which is proportional to the strength of the mixing in (7.23). The oscillation length $L_{osc} =$ is proportional to the neutrino energy E_ν and inversely proportional to the squared mass difference Δm^2.

Neutrino oscillations

Expressed in units suitable for the energy of the atmospheric neutrinos and for the geometry of their detection the oscillation probability is

$$P_{\nu_\alpha \to \nu_\beta} = \sin^2(2\theta) \sin^2 \left(1.27 \frac{\Delta m^2(\mathrm{eV}^2) L_{\mathrm{km}}}{E_{\mathrm{GeV}}} \right) . \qquad (7.25)$$

In neutrino oscillation studies the sensitivity to Δm^2 comes from the L/E ratio while the determination of the mixing strength is a matter of experimental statistics independently of Δm^2.

remarks:

1) **neutrino oscillations require** $m_\nu > 0$

2) **experiments are sensitive to** Δm^2_ν
   not the mass directly

3) **and mixing angle cannot be measured independently**

4) **in optimal case, distance source-detector should be of the order of** L

Neutrino oscillations

Atmospheric neutrinos allow the exploration of a variety of L/E_ν values. Ignoring the depth of the underground detector and assuming that neutrinos are always generated vertically at a constant altitude h one can calculate the range of $L = [2R^2(1-\cos\theta)]^{1/2} + h(\theta)$. Downward-going vertical neutrinos are created at distances h between 10 and 20 km from the detector, while upward-going ones must propagate at distances as large as the Earth's diameter, i.e. of the order of 10^4 km. Since different types of events are generated by neutrinos of energy between 1 and 100 GeV, atmospheric neutrinos can probe L/E_ν from 1 to 10^4 and correspondingly Δm^2 values from 1 to 10^{-4} eV^2. Since the atmospheric neutrino statistics is relatively small, however, only large values of $\sin^2(2\theta)$ can be studied, close to the maximum mixing angle of 45°.

Neutrino oscillations

The physical parameter L/E_ν is a combination of two observable parameters: the neutrino energy deduced from the lepton energy and propagation length, which can be experimentally estimated from the angle of the incoming lepton. The angle between the lepton and the parent neutrino is significant at low energy and decreases as $E_\nu^{-1/2}$ with energy. For the Super-K sub-GeV sample with $\langle E_\nu \rangle$ of 0.77 GeV the average $\cos(\vartheta_{\nu\mu})$ is 0.53. For the multi-GeV sample ($\langle E_\nu \rangle = 5.7$ GeV) $\cos(\vartheta_{\nu\mu}) = 0.97$. At still higher energy, for upward-going neutrino-induced muons, the angle is measured in degrees.

Super Kamiokande

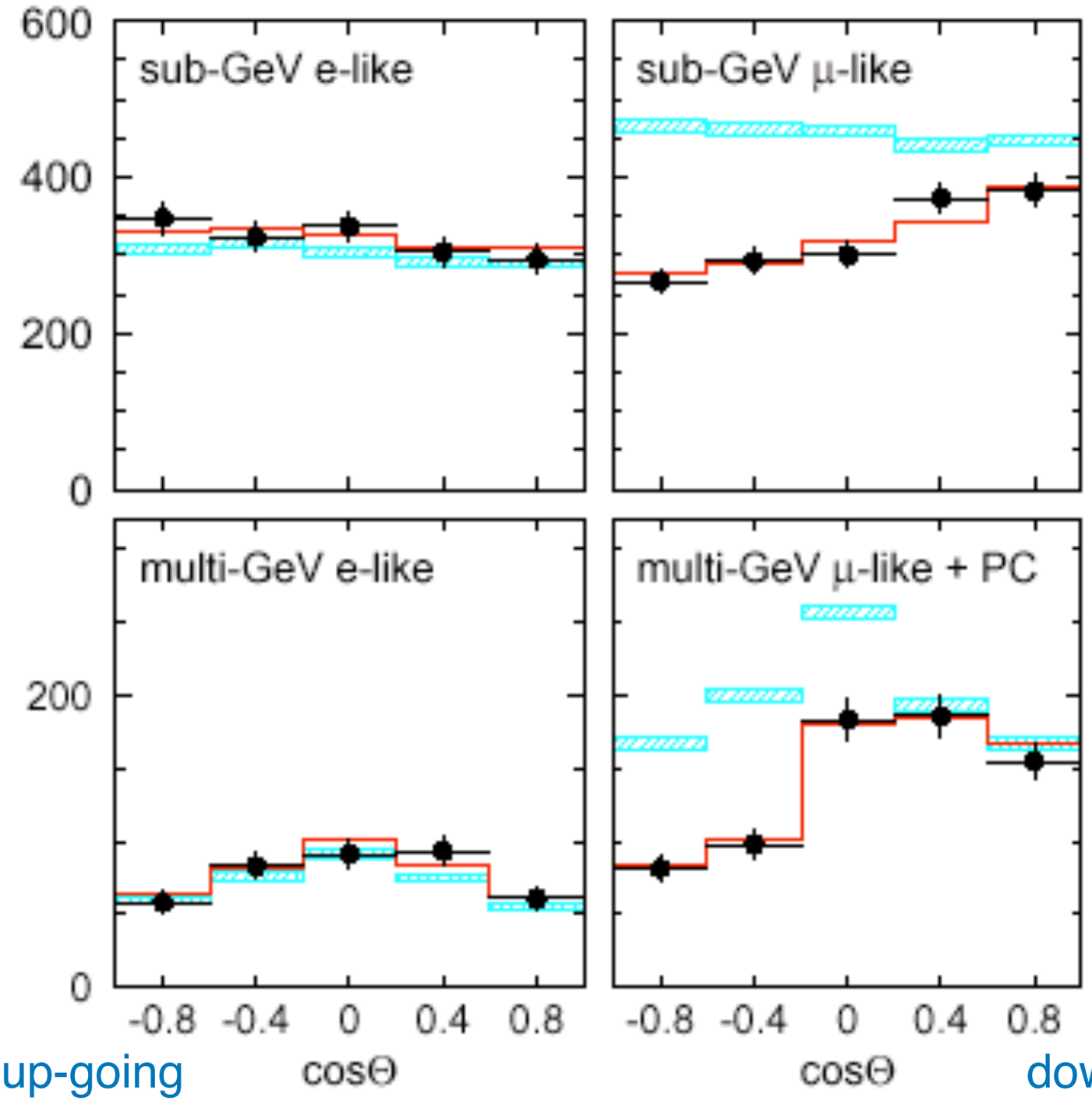

ν_e **experimental results agree with expectations at all angles**

ν_μ **small angles (l ~10-30 km): agreement with expectations large angles (l ~13000 km): experimental data are a factor ~2 less than expectation**

preferred explanation: neutrino oscillations $\nu_\mu \rightarrow \nu_\tau$

best fit values:

$$\sin 2\Theta = 1.0$$

$$\Delta m^2 = 3.5 \cdot 10^{-3}\ \mathrm{eV}^2$$

Angular distributions for *e*-like (left) and m-like (right) events, for sub-GeV (top) and multi-GeV (bottom) samples. The bars show the MC no-oscillation prediction with statistical errors, and the line shows the oscillation prediction for the best-fit parameters, $\sin^2 2\theta = 1.0$ and $\Delta m^2 = 3.5 \times 10^{-3}$ eV^2.

Evidence for neutrino oscillations (Super-Kamiokande @Neutrino '98)

Y. Fukuda et al., PRL 81 (1998) 1562

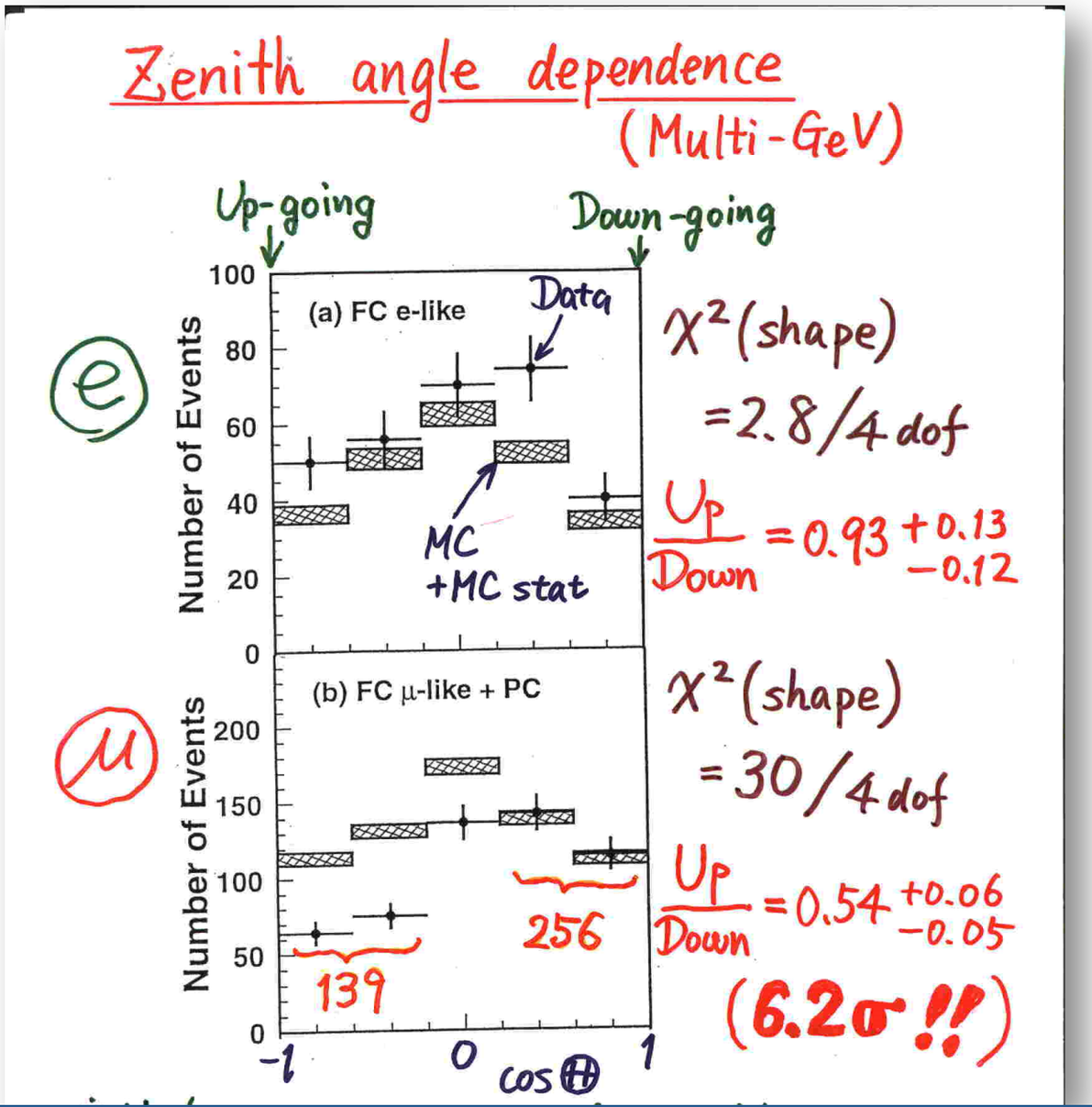

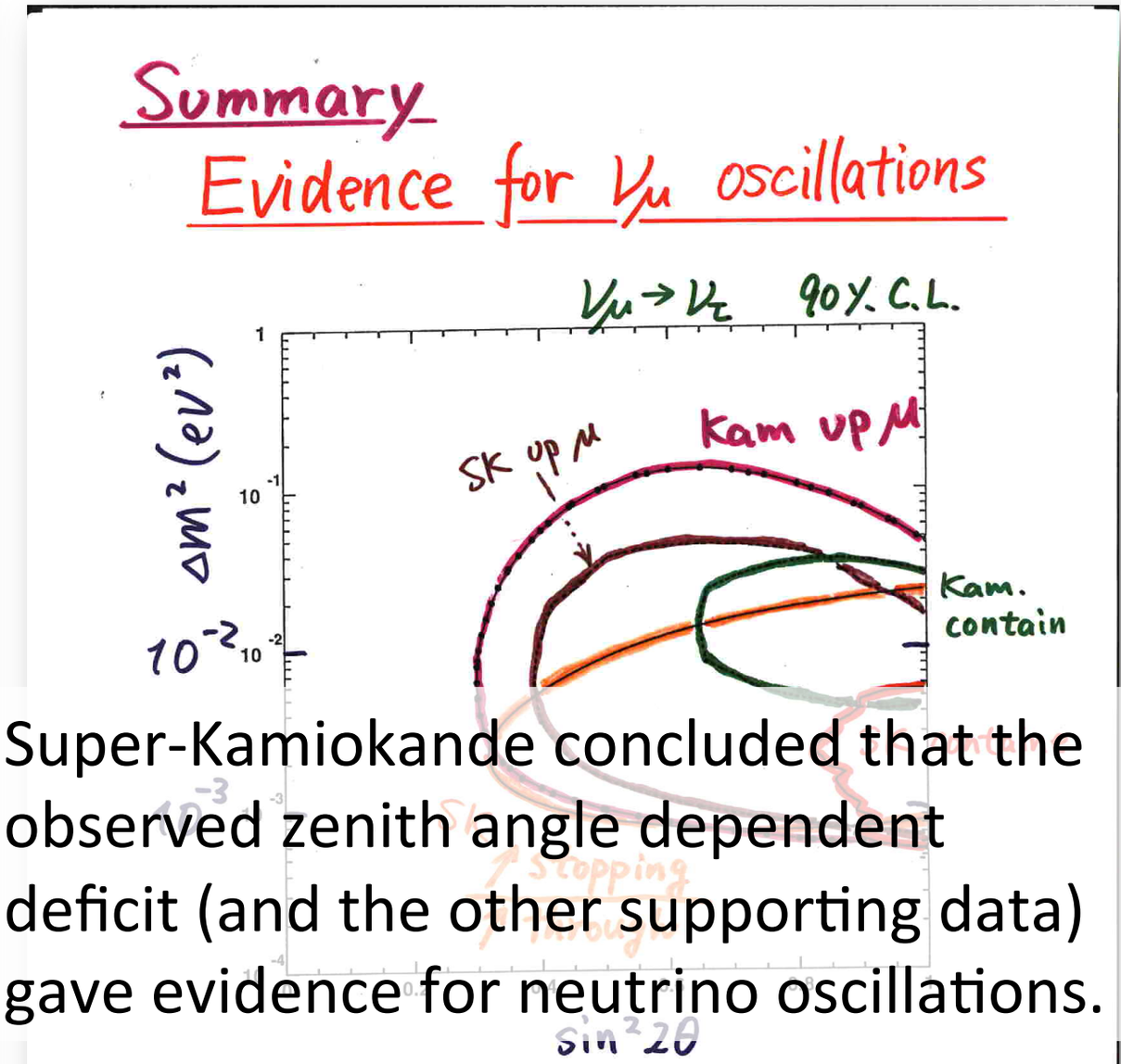

Super-Kamiokande concluded that the observed zenith angle dependent deficit (and the other supporting data) gave evidence for neutrino oscillations.

Neutrino oscillations

To demonstrate the effect I plot in Fig. 7.16 the effect of oscillations with $\sin^2(2\theta) = 1$ and $\Delta m^2 = 0.01$ eV^2 on neutrinos propagating through one Earth radius. The shaded area is the distribution of neutrino energies that initiate partially contained events. Oscillations convert a fraction of these neutrinos into different (non-observable) neutrino flavor as a function of E_ν.

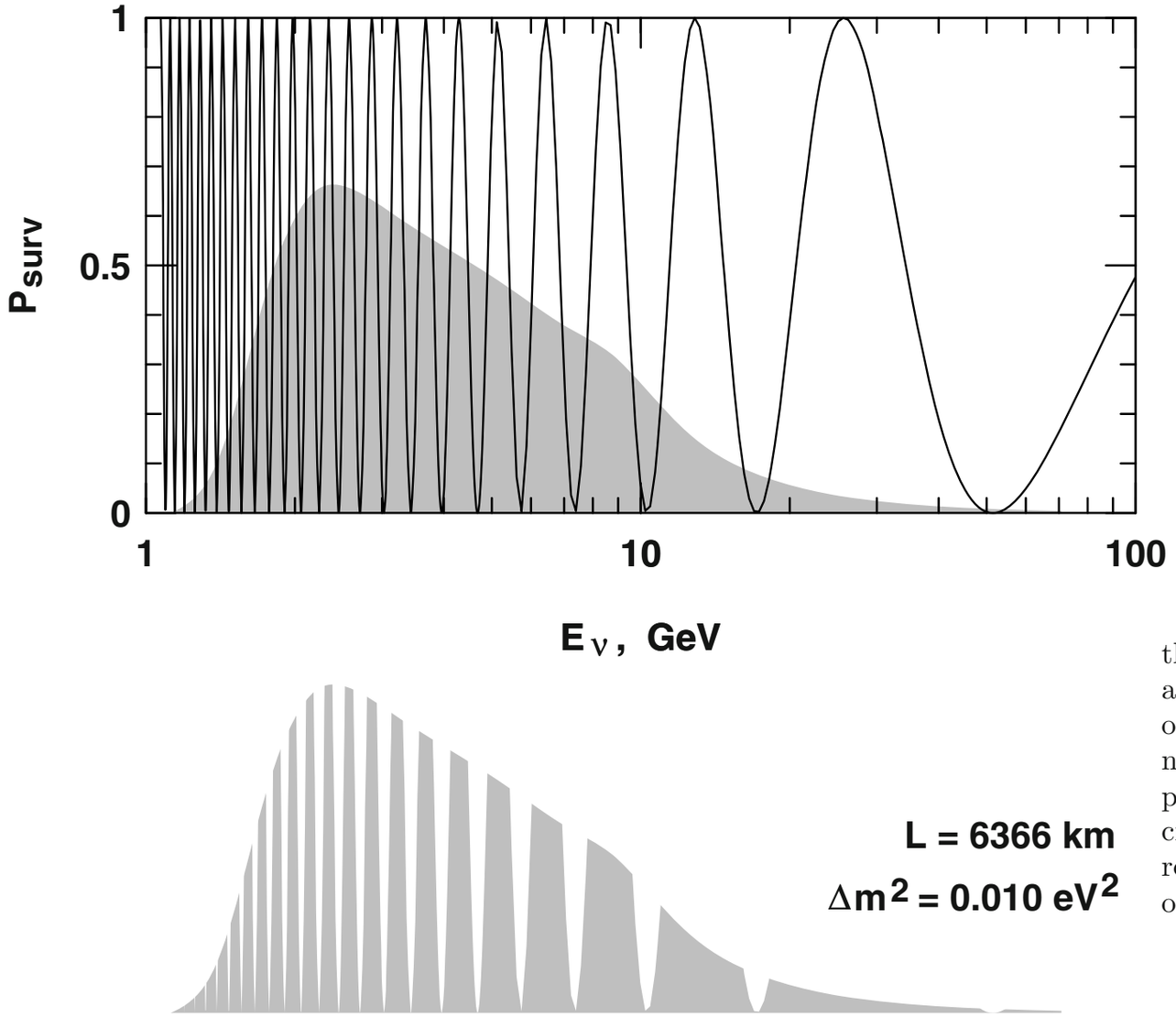

The lower panel of Fig. 7.16 shows what the effect of oscillations is on the rate of neutrino events. A fraction of the parent neutrinos have oscillated according to (7.25) and do not reach the detector. The rate is what remains of the shaded area. It is lower and $R2$ decreases but the value of Δm^2 is not known. For the example neutrino spectrum above Δm^2 of 0.01 and 0.001 produce almost indistinguishable rate decreases. A better derivation of the oscillation parameter space requires a more detailed analysis of the experimental results, such as studies of the angular distribution of the neutrino event rate or, even better, rate vs. L/E plots.

Fig. 7.16. The oscillation probability is plotted as a function of the neutrino energy for propagation on 6,366 km and for Δm^2 of 0.01 eV^2. The shaded area is the energy spectrum of neutrinos responsible for partially contained neutrino events.

What will happen if the ν_μ deficit is due to neutrino oscillations

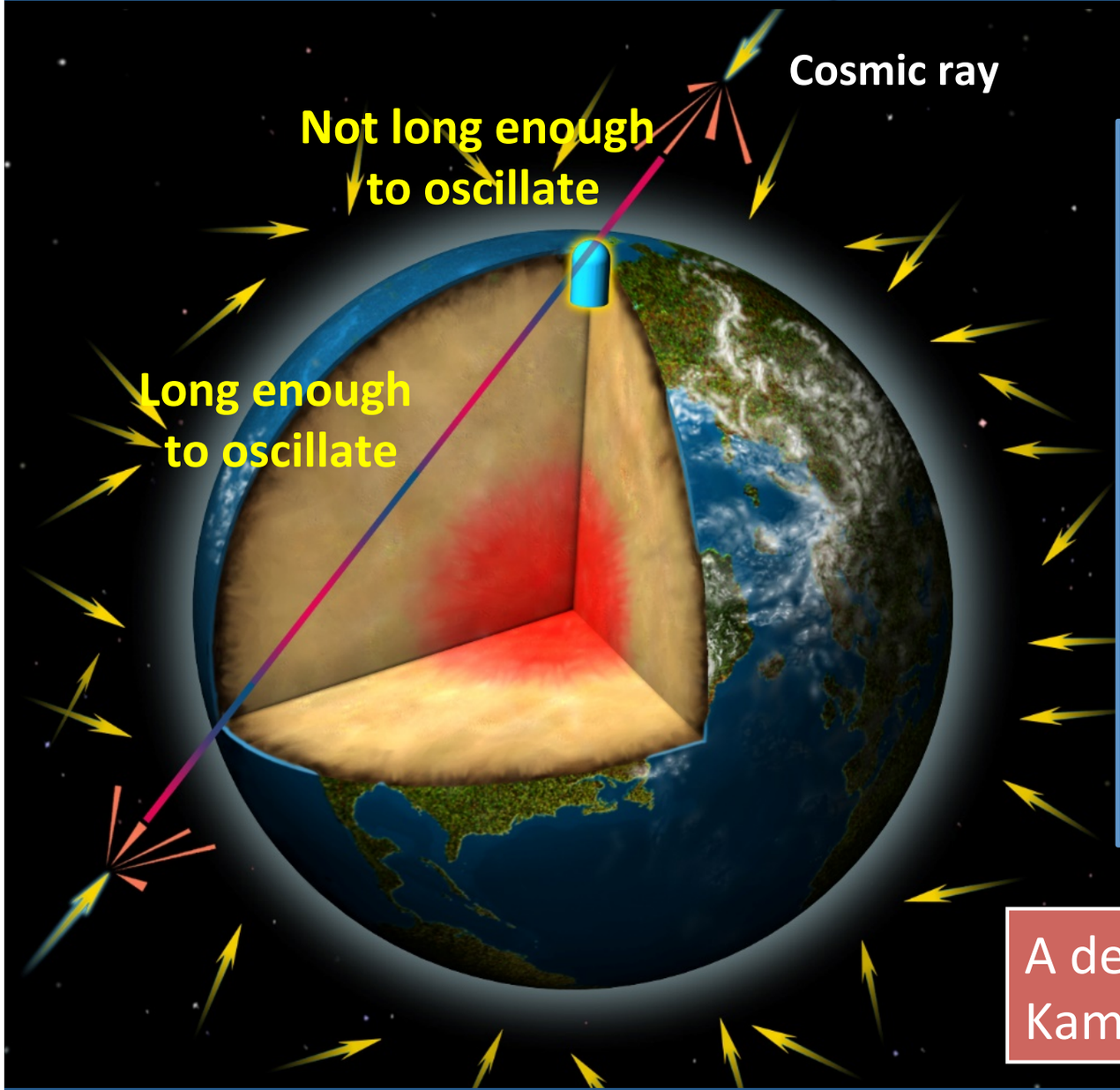

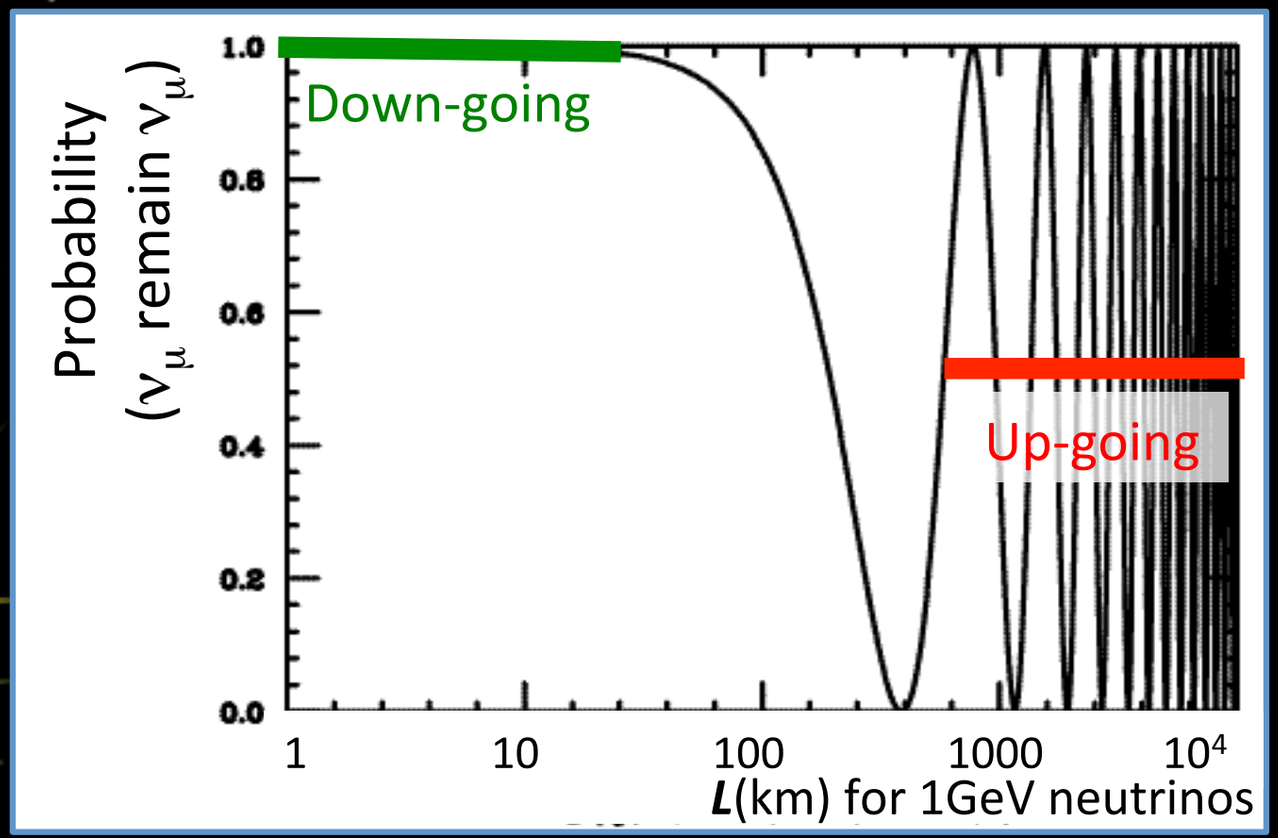

A deficit of upward going ν_μ's should be observed!
Kamiokande was too small. ➔ Super-Kamiokande

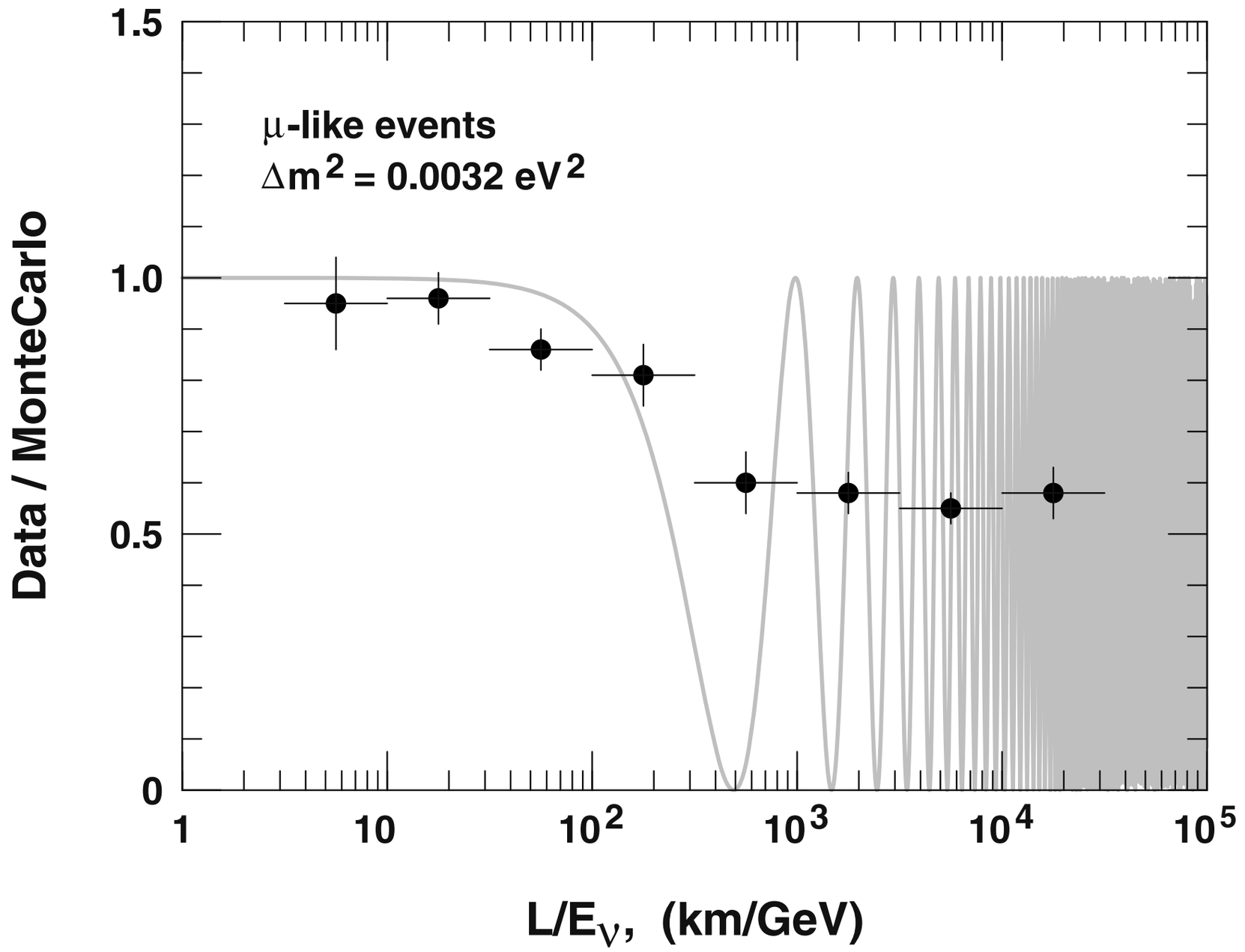

Fig. 7.21. Ratio of data to Monte Carlo predictions for muon events in Super-K. For $\Delta m^2 = 0.0032$ eV^2 the first oscillation minimum is reached at L/E_ν of 500.

Oscillation parameters

atmospheric neutrinos —> study angular distribution of the detected neutrinos as a function of the lepton energy

Figure 7.18 shows the angular distribution of the electron and muon events in two energy ranges – sub-GeV ($E_\nu < 1.33$ GeV) and multi-GeV ($E_\nu > 1.33$ GeV).

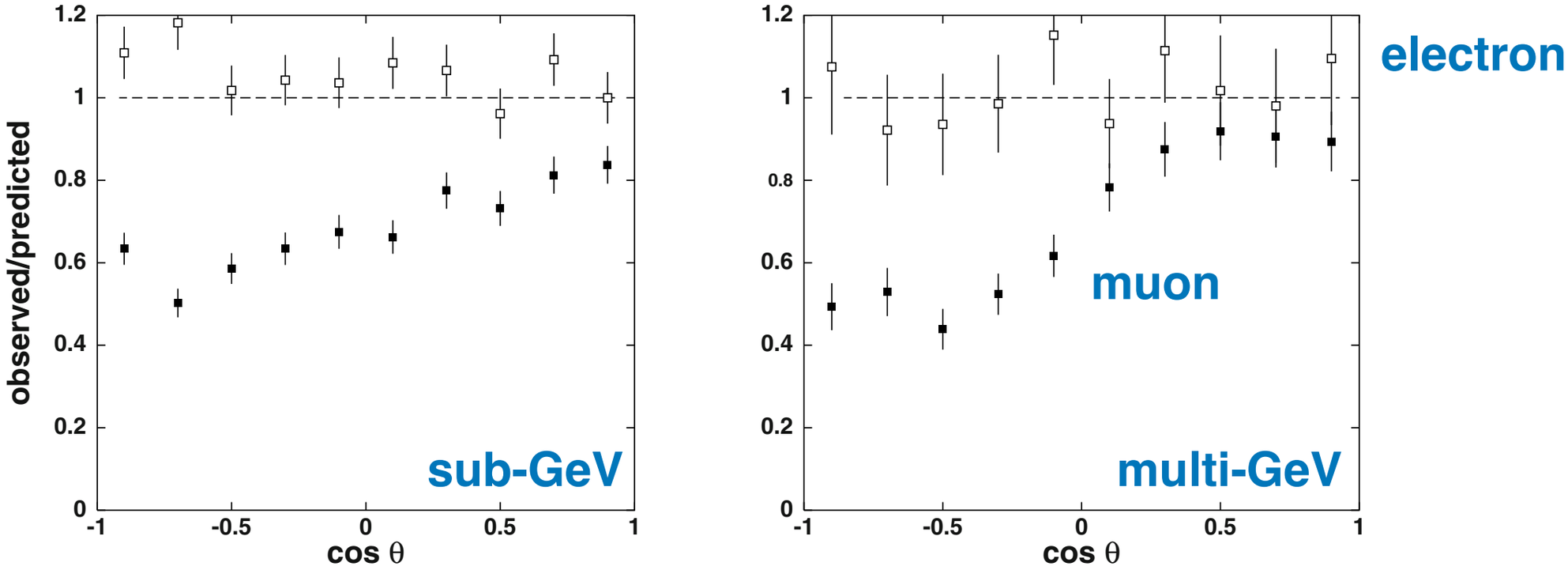

Fig. 7.18. Angular distribution of electron (open symbols) and muon (closed symbols) events in Super-Kamiokande. The points show the ratio between observed and predicted number of events. Left-hand panel is for sub-GeV events and the right-hand panel for multi-GeV events.

The global fit of the Super-K data gives Δm^2 of between 1.5 and 4 $\times 10^{-3}$ eV^2 and $\sin^2 2\theta > 0.9$, i.e. almost maximum mixing angle, for the disappearance of muon neutrinos. The central value of Δm^2 varies between 2.0 and 3.2 $\times 10^{-3}$ eV^2 in slightly different analyses.

atmospheric neutrinos

Oscillation parameters

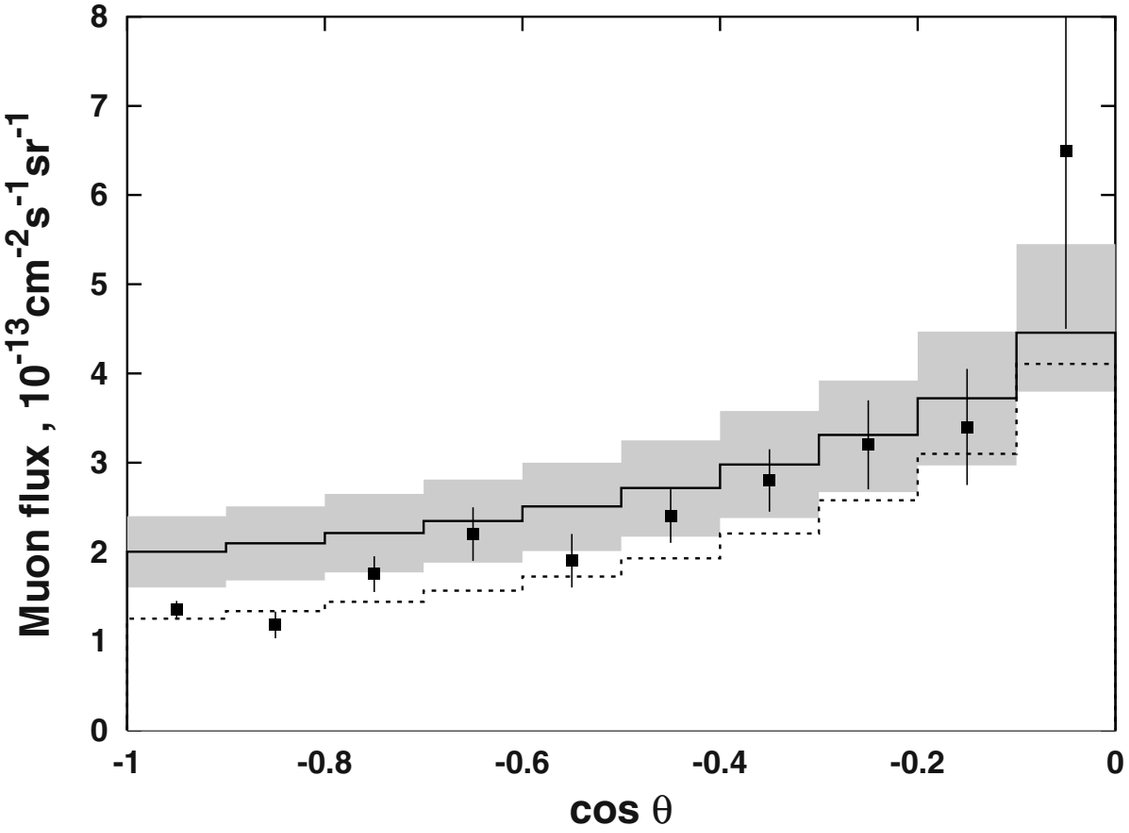

Fig. 7.19. Angular distribution of upward-going neutrino-induced muons (points) in MACRO compared to predictions without (solid histogram) and with (dashed histogram) oscillations.

This result is confirmed by other experiments. Figure 7.19 compares the rate of upward-going muons of energy >1 GeV in MACRO [222] compared to the prediction of Ref. [165]. A theoretical error of $\pm 20\%$ is indicated with a shade. Experimental points for $\cos\theta <$ -0.5 lie well below the predictions. MACRO is 76.6 m long, 12 m wide, and 9.6 m tall. It is highly sensitive to upward-going muons and has almost no efficiency for horizontal events. For this reason the errors for almost horizontal muons are very large. The dashed histogram in Fig. 7.19 is the prediction with the best experimental fit – $\Delta m^2 = 2.5\times10^{-3}$ eV^2 and $\sin^2 2\theta = 1$. The Soudan2 detector fits slightly bigger and less certain $\Delta^2 m$ values, which is consistent with the other results [221].

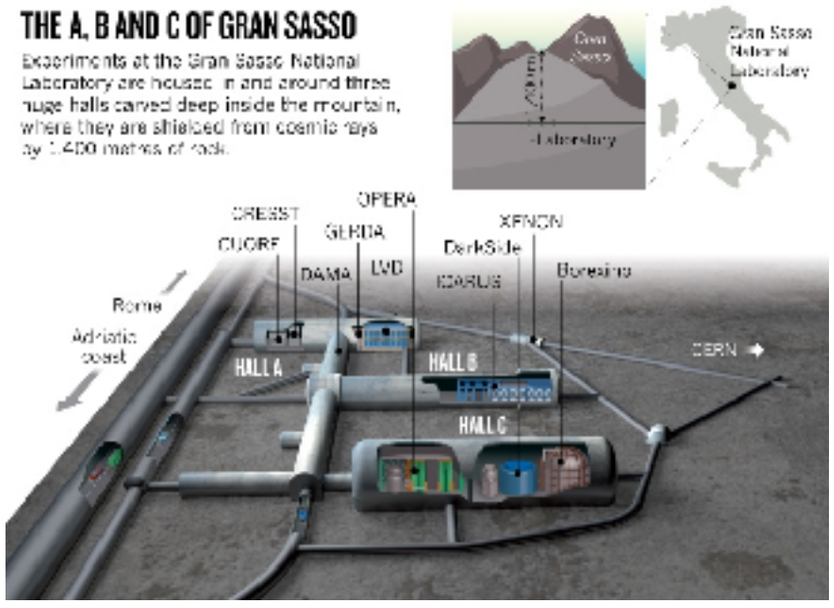

Oscillation parameters

The question of what the disappearing ν_μs become is more complicated. The data shown in Fig. 7.18 exclude a $\mu_\mu \rightarrow \nu_e$ scenario as a major oscillation pattern. The difference between $\nu_\mu \rightarrow \nu_\tau$ and $\nu_\mu \rightarrow \nu_s$ oscillations is in the matter effects. ν_μ and ν_τ have the same effective potential in matter, while ν_ss have $V = 0$. The potential difference $V_{\nu_\mu \nu_s}$ modifies the oscillation pattern and both Super-K [227] and MACRO [228] have reached the conclusion that the oscillations are $\nu_\mu \rightarrow \nu_\tau$.

atmospheric neutrinos

The Nobel Prize in Physics 2002

Raymond Davis Jr., Masatoshi Koshiba, Riccardo Giacconi

- **The Nobel Prize in Physics 2002**
- Nobel Prize Award Ceremony
- Raymond Davis Jr.
- Masatoshi Koshiba
- Riccardo Giacconi

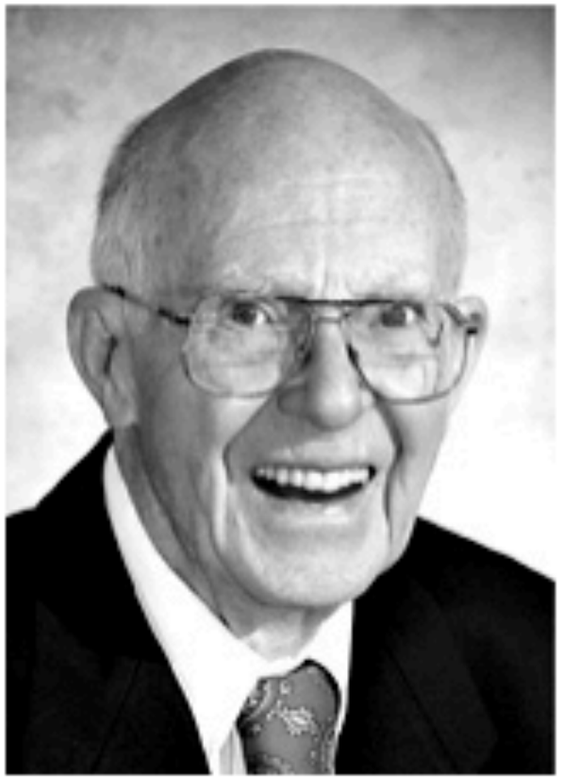

Raymond Davis Jr.

Masatoshi Koshiba

Riccardo Giacconi

The Nobel Prize in Physics 2002 was divided, one half jointly to Raymond Davis Jr. and Masatoshi Koshiba *"for pioneering contributions to astrophysics, in particular for the detection of cosmic neutrinos"* and the other half to Riccardo Giacconi *"for pioneering contributions to astrophysics, which have led to the discovery of cosmic X-ray sources"*.